SLAC – PUB – 3604
March 1985
(T/E)

SEARCHING FOR THE INTERMEDIATE MASS HIGGS BOSON*

JOHN F. GUNION

Physics Department,
University of California, Davis, CA 95616

PAT KALYNIAK

Physics Department,
Carleton University, Ottawa, ON, Canada, K1S 5B6

M. SOLDATE

Stanford Linear Accelerator Center
Stanford University, Stanford, California, 94305

and

PETER GALISON

Physics Department
Stanford University, Stanford, California, 94305

Submitted to *Physical Review D*

---

* Work supported in part by the Department of Energy, contracts DE-AC-3-76SF00515 and DE-AT03-76ER70191.

We study the feasibility of detecting a neutral Higgs boson H^0, with mass between $2m_t \approx 80$ GeV (by assumption) and $2m_W$ at an e^+e^- machine or the SSC. Backgrounds to the production at an e^+e^- machine of H^0 in association with a Z are calculated with particular emphasis on the case when $m_H \approx m_Z$. We present a detailed survey of the signals for and backgrounds to the inclusive or associated production at the SSC of H^0 followed by the decay of H^0 into one of the available channels. There is no signature which is established to be identifiable at the SSC. Only a few signatures remain to be studied, and the further calculations of most immediate interest are pointed out.

I. Introduction

The search for the standard model Higgs boson is one of the most important efforts of present and future accelerators. The standard $SU(2)_L \times U(1)_Y$ model successfully describes the known weak interactions of weak gauge bosons and fermions in terms of a relatively small number of parameters.[1] A critical component of the model is a $SU(2)$ scalar doublet which, through the Higgs mechanism, is responsible for the breaking of the gauge symmetry. A single neutral scalar, the Higgs, remains in the physical spectrum after electro-weak symmetry breaking (EWSB). Experiment, however, has yet to uncover the Higgs.

Though there are a variety of theoretical reasons to suppose that this mechanism is an incomplete description of the nature of EWSB, it remains the standard of comparison for discussions of EWSB. It has the virtue of being the most economical way to give mass to both gauge bosons and fermions. Models,such as technicolor,[2] in which the $W^\pm$ and Z bosons acquire mass through mixing effects involving three scalar Goldstone bosons that are not components of

$SU(2)$ doublets, typically have trouble obtaining fermion masses without encountering problems with, for example, flavor-changing neutral currents.[3] In several extensions of the standard model which are designed to explain some of its apparently arbitrary features, (e.g. SUSY models where supersymmetry breaking occurs near the weak scale,[4] and $SO(18)$[5]) it is necessary that there be more than one $SU(2)$ doublet involved in EWSB. In most such cases there is one neutral scalar similar to the standard Higgs, but with relatively enhanced or diminished couplings to weak gauge bosons and fermions. A good guideline for the phenomenology of such a particle is that of the standard Higgs itself.

Although the couplings of the Higgs to gauge bosons and fermions are prescribed in terms of their own masses, the mass of the Higgs is basically undetermined within the standard model. A lower limit of 7.3 GeV derives from the requirement that higher order corrections to the scalar effective potential do not destroy the symmetry breaking scheme,[6] while an upper limit of order 1 TeV applies if lowest order partial wave unitarity is not to be violated at energies above m_H.[7]

Our purpose in this article is to study the production and observation of a Higgs in the 'intermediate' mass range between, roughly, 90% of the toponium (Θ) mass (80 GeV?) up to twice the W mass. For masses below the lower limit the Higgs can be found in the modes[8]

$$\Theta \to H + \gamma \quad \text{or} \quad Z \to H + \begin{pmatrix} e^+e^- \\ \mu^+\mu^- \end{pmatrix} ,$$

since the backgrounds are controllable with the large numbers of Z's and Θ's soon to be available at planned e^+e^- colliders. A Higgs particle with mass above $2m_W$ can be produced and detected in its W^+W^- or Z^0Z^0 decay mode at high-energy

hadron colliders as discussed , for instance, in Ref. 10. Continuum W^+W^- and Z^0Z^0 pair production is sufficiently small that so long as the Higgs width is not too large a modest pair mass resolution will suppress this background adequately. Some portion of the intermediate mass domain, roughly up to 100 GeV, will be accessible to planned e^+e^- machines where the Higgs can be produced in association with an on-shell Z^0 using[8,9]

$$e^+e^- \rightarrow Z^* \rightarrow Z + H^0$$
$$\hookrightarrow \ell^+\ell^-$$

In this mode an accurate measurement of the momenta of the lepton pair coming from the Z-decay can be used to determine the H mass, thereby avoiding the necessity of a detailed reconstruction of the Higgs decay. Only in the case $m_H \approx m_Z$ could the continuum backgrounds from $Z\ Z^*$ and $Z\gamma^*$ become a significant impediment to the detection of the standard Higgs using this process. We shall consider carefully the case of near degeneracy in Section II of the paper. The continuum backgrounds could become important even for $m_H \not\approx m_Z$ if there are several Higgs doublets. For instance, in models with two Higgs doublets[11] one of the ZZH_i^0 couplings ($i = 1$ to 3) can be much smaller than in the standard model, while the backgrounds are essentially unmodified. Therefore, we also present in Section II continuum backgrounds over a range of H masses.

The planned e^+e^- machines probably will not be capable of producing the Higgs if its mass is above approximately 100 GeV, and thus in Sections III, IV and V we consider techniques for observing it in hadron–hadron collisions. Below $m_H = 2m_W$ the dominant $t\bar{t}$ decay mode of the Higgs makes detection difficult. The inclusive production of the Higgs through gluon fusion $gg \rightarrow H^0 \rightarrow t\bar{t}$ [12]

is swamped by background from continuum $t\bar{t}$ pair production. This is briefly reviewed in Section III. Only associated production of the Higgs with a $t\bar{t}$ pair, another H^0, a Z or a $W^{\pm}$ appears to offer any possibility for detecting H^0 in the $t\bar{t}$ decay mode. Of these the last is most promising, as discussed also in Section III, and is thoroughly studied in Section IV. We show there that the $H^0 + W^{\pm}$ production mode is practical provided adequate mass resolution and b/t quark discrimination is available. Current assessments of detector resolution and jet reconstruction suggest that these criteria will not be easily achievable. Therefore in Section V we consider possibilities for detecting the H^0 in any of several rare decay modes: $\tau^+\tau^-$, L^+L^- where L is a heavy lepton, $W+W^*$, $Z+Z^*$, $\Theta+\gamma$, $Z+\gamma$ and $\gamma+\gamma$. We find that rates appear to be adequate in most cases and that calculations or rough estimates of background are not overwhelmingly discouraging in some cases. The detailed background calculations of most immediate interest are pointed out.

II. Production of H^0 in e^+e^- Collisions

In this section we consider the backgrounds to the production of the intermediate mass Higgs through the process $e^+e^- \rightarrow Z^* \rightarrow ZH^0$ [8,9] (Fig. 1a), considered to be the best reaction for detection of an intermediate mass Higgs at an e^+e^- machine. The Higgs in this mass range decays almost exclusively into $t\bar{t}$. The direct physics background then arises from the continuum production of $e^+e^- \rightarrow Zt\bar{t}$, graphs for which are illustrated in (Fig. 1b). The background is largest for $m_H \approx m_Z$, when it is dominated by

$$e^+e^- \rightarrow ZZ^*$$
$$\qquad\quad \hookrightarrow t\bar{t}\,.$$

We have obtained an analytic result for the contribution of the two graphs of this type. Beyond the case of near degeneracy, it is necessary to compute eight Feynman diagrams to arrive at an accurate estimate of the background. We have performed the complete calculation of the matrix element–squared using REDUCE and have integrated over phase space using Monte Carlo techniques for fixed resolution Δs_H in the $t\bar{t}$ invariant mass-squared $s_H = (p_t + p_{\bar{t}})^2$. The same calculations can be used to estimate possible backgrounds from $e^+e^- \to Zq\bar{q}$, $q = u,\ d,\ c,\ s,$ or b, which are of interest if $t\bar{t}$ pairs cannot be discriminated completely from lighter quark pairs.

Following the conventions of Ref. 13, we define Z couplings to fermions as

$$\begin{pmatrix} g_V^i \\ g_A^i \end{pmatrix} = 2^{1/4}\, m_Z\, \sqrt{G_F}\, \begin{pmatrix} a_i \\ b_i \end{pmatrix} \qquad (II.1)$$

with

$$a_e = -\frac{1}{2} + 2x_W, \quad a_u = a_c = a_t = \frac{1}{2} - \frac{4}{3}x_W, \quad a_d = a_s = a_b = -\frac{1}{2} + \frac{2}{3}x_W$$

$$b_e = b_d = b_s = b_b = -\frac{1}{2}, \quad b_u = b_c = b_t = \frac{1}{2}, \qquad (II.2)$$

and $x_W = \sin^2\theta_W \approx .22$, $m_Z = 93$ GeV. We also define $g_W = \sqrt{8m_W^2 G_F/\sqrt{2}}$. The momenta of the e^-, e^+, Z, t, and $\bar{t}$ are k_1, k_2, q, p_1, and p_2 respectively. We also define

$$s_H = (p_1 + p_2)^2 \qquad (II.3a)$$

$$s = (k_1 + k_2)^2 \qquad (II.3b)$$

$$t = (k_1 - q)^2 \qquad (II.3c)$$

$$u = (k_2 - q)^2 \qquad (II.3d)$$

$$w = \frac{1}{2}(p_1 - p_2) \cdot q \qquad (II.3e)$$

$$v = \frac{1}{2}(p_1 - p_2) \cdot (k_1 - k_2) \qquad (II.3f)$$

$$\beta_t(x) = \sqrt{1 - \frac{4m_t^2}{x}} \qquad (II.3g)$$

$$\alpha_{\pm}^{e} = (g_V^e \mp g_A^e)^2 \qquad (II.3h)$$

$$D_Z(x) = \frac{1}{(x - m_Z^2)^2 + m_Z^2 \Gamma_Z^2} \ . \qquad (II.3i)$$

We will limit our discussion of the cross sections to results of a complete phase space integration with resolution Δs_H in s_H. It is convenient to define

$$\Sigma(s_0,\ \Delta s_H) = \int_{s_0 - \frac{\Delta s_H}{2}}^{s_0 + \frac{\Delta s_H}{2}} ds_H \ \frac{d\sigma}{ds_H} \ . \qquad (II.4)$$

The following integral arises frequently in this context:

$$I_1(\epsilon,\ s_0 - m^2,\ \Delta s) = \int_{s_0 - \frac{\Delta s}{2}}^{s_0 + \frac{\Delta s}{2}} ds \ \frac{1}{(s - m^2)^2 + \epsilon^2}$$

$$= \frac{1}{\epsilon} \left\{ \tan^{-1} \left[\frac{1}{\epsilon} \left(s_0 - m^2 + \frac{\Delta s}{2} \right) \right] - \tan^{-1} \left[\frac{1}{\epsilon} \left(s_0 - m^2 - \frac{\Delta s}{2} \right) \right] \right\} \ . \qquad (II.5)$$

Let us first turn to the analytic result for the signal

$$e^+e^- \to Z H^0$$
$$\qquad\qquad \hookrightarrow t\bar{t} \ .$$

The standard expression for the average invariant matrix element squared is

$$\frac{1}{4}\sum_{\substack{\text{spin, color,}\\ \text{helicity}}}|\mathrm{M}_{Fig.1a}|^2 = \frac{g_W^4 N_C}{\cos^4\theta_W}\, m_t^2\, \left[(g_V^e)^2+(g_A^e)^2\right]\, \frac{1}{(s-m_Z^2)^2}$$
$$\frac{1}{(s_H-m_H^2)^2+m_H^2\Gamma_H^2}\, \left(k_1\cdot k_2+\frac{2q\cdot k_1 q\cdot k_2}{m_Z^2}\right)(p_1\cdot p_2-m_t^2)\ . \qquad (II.6)$$

Using Eq. (II.4) and Eq. (II.6), one finds

$$\Sigma_{SIG}(s_0,\Delta s_H) = \frac{\pi\alpha^2}{24}\, \left(\frac{2|\vec{q}|}{\sqrt{s}}\right)\, \frac{|\vec{q}|^2+3m_Z^2}{(s-m_Z^2)^2}\, I_1(\Gamma_H m_H,\ s_0-m_H^2,\ \Delta s_H)$$
$$\frac{1-4x_W+8x_W^2}{x_W^2(1-x_W)^2}\, \frac{m_H\Gamma_{H\to t\bar{t}}}{\pi}\, \frac{s_0}{m_H^2}\, \left[\frac{\beta_t(s_0)}{\beta_t(m_H^2)}\right]^3 \qquad (II.7)$$

where $|\vec{q}| = \sqrt{\frac{1}{4}s-\frac{1}{2}(s_0+m_Z^2)+(s_0-m_Z^2)^2/(4s)}$ is the center of mass Z momentum at $s_H = s_0$, and I_1 was defined in Eq. (II.5). The background arising from

$$e^+e^- \to ZZ^*$$
$$\qquad\qquad \hookrightarrow t\bar{t}$$

is obtained from the two diagrams of Fig. 2. In the notation of Eq. II.3(a–f),

$$\frac{1}{4}\sum_{\substack{\text{spin, color,}\\ \text{helicity}}} |\mathrm{M}_{Fig.2a} + \mathrm{M}_{Fig.2b}|^2 =$$

$$D_Z(s_H)\ N_C \left\{ -2(\alpha_+^{e2} + \alpha_-^{e2}) \left[s_H(g_V^{t2} + \beta_t^2(s_H) g_A^{t2}) \right.\right.$$

$$\left[m_Z^2\ s_H \left(\frac{1}{u^2} + \frac{1}{t^2}\right) - \frac{t}{u} - \frac{u}{t} - \frac{2s(m_Z^2 + s_H)}{tu} \right]$$

$$+ (g_V^{t2} + g_A^{t2}) \Big\{ 2 \left[m_Z^2 \left(\frac{1}{u^2} + \frac{1}{t^2}\right) - \frac{2s_H}{tu} \right] (w^2 + v^2) - 4\frac{m_Z^2}{tu}\ (w^2 - v^2)$$

$$+ 4wv\ m_Z^2 \left(\frac{1}{u^2} - \frac{1}{t^2}\right) - (4m_t^2 - s_H) \left[\frac{ut - m_Z^2 s_H}{2}\ \left(\frac{1}{u^2} + \frac{1}{t^2}\right) + \frac{s s_H}{tu} \right] \Big\} \Big]$$

$$- 8(\alpha_+^{e2} - \alpha_-^{e2}) g_V^t g_A^t\ s_H$$

$$\left\{ w \left[m_Z^2 \left(\frac{1}{u^2} - \frac{1}{t^2}\right) + \frac{1}{t} - \frac{1}{u} \right] + v \left[m_Z^2 \left(\frac{1}{t^2} + \frac{1}{u^2}\right) - \frac{1}{t} - \frac{1}{u} - \frac{2s}{tu} \right] \right\} \Bigg\} \tag{II.8}$$

If the $t\bar{t}$ phase space integral is performed at fixed s_H with no other restrictions, the terms of Eq. (II.8) linear in w and v vanish by symmetry. The result of the complete phase space integration of Eq. (II.8) as specified by Eq. (II.4) is

$$\Sigma_{BG}^{Z-pole}\ (s_0,\ \Delta s_H) = \frac{1}{2(2\pi)^3}\ (\alpha_-^{e2} + \alpha_+^{e2}) \left[s_0\ (g_V^{t2} + g_A^{t2}) + 2m_t^2\ (g_V^{t2} - 2g_A^{t2}) \right]$$

$$\frac{\beta_t(s_0)}{s}\ I_1\left[\Gamma_Z m_Z,\ s_0 - m_Z^2,\ \Delta s_H\right]$$

$$\left\{ \frac{1}{2} \left[\frac{1 + \frac{(m_Z^2 + s_0)^2}{s^2}}{1 - \frac{(m_Z^2 + s_0)}{s}} \right]\ \ell n\ \left[\frac{(1 + \tilde{\beta}_Z)^2 - \left(\frac{m_Z^2 - s_0}{s}\right)^2}{(1 - \tilde{\beta}_Z)^2 - \left(\frac{m_Z^2 - s_0}{s}\right)^2} \right]\ - \tilde{\beta}_Z \right\} \tag{II.9}$$

where

$$\tilde{\beta}_Z = \sqrt{\left(1 + \frac{m_Z^2 - s_0}{s}\right)^2 - \frac{4m_Z^2}{s}} \,. \qquad (II.10)$$

One may check Eqs. (II.9) and (II.10) in the narrow width approximation, $\frac{\Gamma_Z m_Z}{\Delta s_H} \to 0$, by comparison to the standard calculation of $e^+e^- \to Z^0 Z^{013}$ provided Γ_Z is set to $\Gamma_{Z \to t\bar{t}}$ (since only the $t\bar{t}$ mode appears in the above calculation).

Before proceeding to compare Σ_{BG}^{Z-pole} and Σ_{SIG}, we must consider the possible interference of background amplitudes with the signal amplitude. Consider the overlap between the two diagrams of Fig. 2 and the signal diagram of Fig. 1a. This interference amounts to considering the real cuts of $t\bar{t}$ loop insertions that mix the Higgs and Z propagators. The full $t\bar{t}$ phase space integral of such an insertion must vanish by gauge invariance which prohibits HZ mixing. In actual calculations the interference term, $M_{Fig.2a\ \&\ Fig.2b} \cdot M_{signal}$, is proportional to v and w of Eq. (II.3 e, f), which vanish when integrated over $t\bar{t}$ phase space. Certain types of experimental cuts would, of course, allow non-zero interference terms. However, aside from $M_{Fig.2a\ \&\ Fig.2b} \cdot M_{signal}$ being proportional to w and v this interference is also proportional to g_V^e. This is to be compared to $|M_{Fig.2a\ \&\ Fig.2b}|^2$, which is proportional to g_A^e; since $g_V^e/g_A^e \approx \frac{1}{10}$, such terms are small.

When comparing the signal to the background in the case of near degeneracy it is important to take into account the relative sizes of Δs_H and the widths, Γ_H and Γ_Z. The typical resolution Δs_H in the s_H variable is determined by the measurement error of the trigger Z^0 momentum. Assuming 1% accuracy in measuring the e^+ or e^- momenta from the trigger Z^0 decay, we would obtain a

2% error in s_H, i.e.

$$\frac{\Delta s_H}{s_0} \approx .02 \ . \qquad (II.11)$$

This exceptional resolution is projected for the LEP 3 detector.[14]

The Higgs width in the intermediate mass range is dominated by the contribution from the $t\bar{t}$ mode except when m_H is very close to $2m_t$ or $2m_W$.

$$\Gamma_{H\to t\bar{t}} = \frac{N_C}{8}\,\frac{g_W^2}{4\pi}\,\left(\frac{m_t}{m_W}\right)^2\,\left(1-\frac{4m_t^2}{m_H^2}\right)^{3/2}\,m_H \qquad (II.12)$$

For $m_t = 40$ GeV, $\Gamma_{H\to t\bar{t}}$ takes the values

$$\Gamma_{H\to tt} \approx \begin{cases} 70 \text{ MeV} & m_H = 100 \text{ GeV} \\ 150 \text{ MeV} & m_H = 120 \text{ GeV} \\ 350 \text{ MeV} & m_H = 160 \text{ GeV} \end{cases} , \qquad (II.13)$$

and $m_H\Gamma_H$ is small compared to expected values of Δs_H. The narrowness of the signal is illustrated in Fig. 3a where we plot $\Sigma_{SIG}(s_0, \Delta s_H)$ as a function of $\sqrt{s_0}$ assuming $m_H = m_Z$. In contrast, for $\sqrt{s_0} \approx 100$ GeV, Δs_H and $m_Z\Gamma_Z$ are comparable, and the integral I_1 of Eq. (II.9) will exhibit nontrivial behavior depending upon the value of s_0.

To compare the signal and the approximate background, we choose a value of m_H and compare $\Sigma_{SIG}(s_0 = m_H^2, \Delta s_H)$ and $\Sigma_{BG}^{Z-pole}(s_0 = m_H^2, \Delta s_H)$ for m_H near m_Z. The accuracy of neglecting the other contributions to the background in the case of near degeneracy will become apparent later in this section when the complete background is discussed for arbitrary m_H. Fig. 3b summarizes our results. It contains $\Sigma_{BG}^{Z-pole}\ (s_0, \Delta s_H)$ and $\Sigma_{SIG}(s_0, \Delta s_H)\Big|_{m_H=\sqrt{s_0}}$. In other words, the signal curve of Fig. 3b, at a particular value of $\sqrt{s_0}$, is the maximum

possible Higgs signal at that $\sqrt{s_0}$, and is obtained by choosing $m_H = \sqrt{s_0}$; e.g. the signal of Fig. 3a where $m_H = m_Z$ is represented in the signal curve of Fig. 3b by the point at $\sqrt{s_0} = m_Z$. In a plot of an experimentally determined $\Sigma(s_0, \Delta s_H)$ one should see a superposition of the appropriate background curve from Fig. 3b with a signal such as Fig. 3a centered about $\sqrt{s_0} = m_H$.

From Figs. 3a and 3b one can conclude the following. If the $t\bar{t}$ jets can be distinguished from light quark pair jets, Σ_{BG}^{Z-pole} is always well below the signal of a conventional Higgs. In the other extreme where the $t\bar{t}$ jets are indistinguishable experimentally from light quark jets, one must sum over $\bar{q}q$ modes in $e^+e^- \to Zq\bar{q}$ to obtain the complete background. Fig. 3b shows that if $m_H = m_Z$ the background and signal are then approximately equal. Even in this extreme the background falls rapidly relative to the signal as $|m_H - m_Z|$ increases. It is apparent that with high resolution in s_H there exists a motivation to discriminate between t and other quark jets only when searching for a standard Higgs with mass within about 1 GeV of m_Z.

As mentioned previously we have also carried out a complete calculation of the background cross section arising from all the diagrams of Fig. 1b. Away from $\sqrt{s_0} = m_Z$, Σ_{BG}^{Z-pole} is no longer a good approximation to the background. While for cases when m_H is not near m_Z the total background would be negligible in the simplest one-doublet Higgs model, it could become a significant factor in searching for neutral scalars with ZZ couplings smaller than the standard model value. For example weakly coupled Higgses are found in some two-dublet models; see for instance the minimal SUSY two-doublets results of Ref. 15.

The complete background calculation is tedious and will not be discussed in detail. We confine ourselves to a discussion of the accuracy of our calculation,

and a presentation of numerical results for $\Sigma_{BG}(s_0, \Delta s_H)$, the total background cross-section.

We wish to compute $\Sigma_{BG}(s_0, \Delta s_H)$. Away from $m_H = m_Z$ the only subtle integrations in calculating $\Sigma_{BG}(s_0,\ \Delta s_H)$ are of the form

$$\int_{s_0 - \frac{\Delta s_H}{2}}^{s_0 + \frac{\Delta s_H}{2}} ds_H \, \frac{(s_H - m^2) f(s_H)}{(s_H - m^2)^2 + \epsilon^2} \, .$$

Such an integration is not necessarily computed accurately by a Taylor expansion of $f(s_H)$ about s_0. When $s_0 = m_H^2$ the leading term vanishes. Nonetheless, we have approximated the full background contribution by taking $f(s_H) \approx f(s_0)$ even at $s_0 = m_H^2$, and have estimated that the sum of neglected terms is no larger than the sum of the terms in the background which we have calculated explicitly.

In Fig. 4a we plot the sum of background terms ignoring interference between background and signal (along with a comparison to the contribution arising only from the $Z-pole$ terms) for $t\bar{t}$, $b\bar{b}+t\bar{t}$, and all $q\bar{q}$. We take Δs_H according to Eq. (II.11). This full background should be used by superimposing an appropriate Higgs signal centered at $\sqrt{s_0} = m_H$. For full strength ZZH coupling we plot in Fig. 4b the peak signal value $\Sigma_{SIG}(s_0 = m_H^2,\ \Delta s_H = .02\ m_H^2)$. Clearly for full strength coupling the background is negligible. If the coupling strength were reduced then peak signal and background could become comparable. For example with a $t\bar{t}$ trigger a reduction factor of $\sim 10^{-3}$ in $|g_{ZZH}|^2$ would make background and signal equal. Only in this latter situation of weak ZZH coupling is the background likely to be a problem if the resolution of Eq. (II.11) can be achieved.

As stated, the above procedure ignores the interference terms. These are never of importance. We demonstrate this in Fig. 5 where we plot for $m_H = 130$ GeV the absolute value of the interference contribution to the full cross section in comparison to the purely background contribution. This plot is for the pure $t\bar{t}$ trigger case for which the interference is relatively largest. We see that in the region $\sqrt{s_0} \approx m_H$, where the signal is large compared to background, the interference term can be of order 30% of the purely background terms; but neither are of importance relative to the signal (see Fig. 4b). Away from $\sqrt{s_0} = m_H$ where the signal is small, the interference terms are negligible compared to the pure background contributions. This last statement also applies at $\sqrt{s_0} = m_H$ if the signal is reduced to the size of the background by a nonstandard coupling.

To summarize we can imagine four distinct situations:

(a) signal full strength coupling, $m_H \simeq m_Z$;

(b) signal full strength coupling, $m_H \not\simeq m_Z$;

(c) signal strength substantially reduced, $m_H \simeq m_Z$;

(d) signal strength substantially reduced, $m_H \not\simeq m_Z$; In case (a) Fig. 3b shows that a clean separation of signal from background may require separation of $Zt\bar{t}$ from other $Zq\bar{q}$ channels. In case (b) background should present no problem even if all $Zq\bar{q}$ channels are included. In case (c) one may have difficulty observing the Higgs even with $Zt\bar{t}$ separation. In case (d) $Zt\bar{t}$ separation should, barring extreme signal reduction, enable the

$$ZH \\ \llcorner\!\!\rightarrow t\bar{t}$$

signal to be observed.

III. Overview of H^0 Production in Hadronic Collisions with $H \to t\bar{t}$

We have already observed that planned e^+e^- machines may not probe Higgs masses above $\sim$ 100 GeV, whereas hadronic machines such as the SSC have acceptable absolute rates for Higgs production, even in association with a W or Z, throughout the intermediate mass range (and well beyond it). Below $2m_W$ it is well known that the process (Fig. 6a)

$$pp \to H \to t\bar{t} \qquad (III.1)$$

is swamped by the continuum background from (Fig. 6b)

$$pp \to t\bar{t} \quad . \qquad (III.2)$$

In EHLQ,[10] for instance, we find at $\sqrt{s} = 40$ TeV that the Higgs cross section is

$$\sigma_H^{t\bar{t}}(m_H = 130 \text{ GeV}) = .1 \ nb \ , \qquad (III.3)$$

whereas the background from (III.2) is ($m_t = 45$ GeV)

$$\frac{d\sigma_{BG}^{t\bar{t}}}{dM}(M = 130 \text{ GeV}) \approx \frac{2nb}{\text{GeV}} \ . \qquad (III.4)$$

In both cross sections the rapidities of the t and $\bar{t}$ are constrained to $|y_t|, \ |y_{\bar{t}}| < 1.5$. Assuming a 5% mass resolution in the $t\bar{t}$ pair mass (an optimistic guess) one finds

$$\frac{\sigma_H^{t\bar{t}}}{\Delta M \frac{d\sigma_{BG}^{t\bar{t}}}{dM}} \ (M = 130 \text{ GeV}) \approx .8 \times 10^{-2} \ , \qquad (III.5)$$

an unacceptably small signal to background ratio, even with 10^6 signal events at integrated luminosity of $10^{40}/cm^2$.

Of course, it is also possible to consider rarer decay modes of the H such as $\tau^+\tau^-$, WW^*, $Z^0\gamma\ldots$, and to estimate corresponding backgrounds. This topic will be discussed in Sec. V where we demonstrate that such modes generally at least have sufficient raw event rate. It is then a question of backgrounds. For the moment, however, we continue to focus on the $t\bar{t}$ decay mode of H.

Given the result Eq. (III.5) it is necessary to turn to associated production of the Higgs, if it is to be observed in its $t\bar{t}$ decay mode. In this section we shall focus on the production of H^0 with a W, Z, or $t\bar{t}$ pair. We omit consideration of the production of two Higgses. This has been estimated in Ref. 10. Due to the absence of a ZH^0H^0 coupling, the H^0–pair event rate is too small to yield a useful event rate; only in a two–doublet model with tree level $ZH^0H^{0\prime}$ couplings could such a signature possibly be usable.

We first focus on

$$\begin{array}{l} pp \to H + t\bar{t} \\ \qquad\quad \hookrightarrow t\bar{t} \end{array} \quad . \tag{III.6}$$

This has been considered by Kunszt[16] with the conclusion that the mode is not practical due to the large QCD backgrounds combined with combinatorical problems in isolating the $t\bar{t}$ that happen to come from the H decay. We remark here that $Ht\bar{t}$ production with H decay into a rarer mode might prove more tractable. We will return to this question in Sec. V.

Next we wish to discuss[17]

$$\begin{array}{l} pp \to H + Z \\ \qquad\quad \hookrightarrow t\bar{t} \end{array} \quad . \tag{III.7}$$

In Fig. 7a we draw the diagram responsible for (III.7) and in Fig. 7b we draw

representative diagrams yielding the background

$$pp \to Z\ t\bar{t}\ . \tag{III.8}$$

The largest contribution to (III.8) derives from gluon-gluon initiated processes. We shall compute in Sec. IV the analogous reaction of (Fig. 8a)[17]

$$\begin{array}{c} pp \to W^+ H \\ \qquad\quad \big\lfloor\!\!\rightarrow t\bar{t} \end{array} \tag{III.9}$$

and the background from (Fig. 8b)

$$pp \to W^+\ t\bar{t}\ . \tag{III.10}$$

As we will show in Sec. IV, the signal to background ratio, ignoring detector questions, is just sufficient for H detection to be possible. However (III.10) receives no contributions from gluon-gluon initiated processes due to the presence of the charge of the W^+H^0 final state. It is well known that gluon-gluon luminosities at the relevant subprocess energies of

$$\hat{s} \gtrsim\ (m_H + m_Z)^2 \tag{III.11}$$

are enormously larger than quark-antiquark luminosities. For instance EHLQ[10] obtains

$$\frac{\tau}{\hat{s}}\ \frac{d\mathcal{L}}{d\tau} = \begin{cases} 80\ \text{nb} & u\bar{u} \\ 8000\ \text{nb} & gg \end{cases} \tag{III.12}$$

at $\hat{s} = (m_H + m_Z)^2$ with $m_H = 130$ GeV. Thus, the background (III.8) would be much larger than the signal (III.7). This coupled with difficulty in reconstructing the H in the $t\bar{t}$ channel makes the mode (III.7) unpractical.

The potentially favorable signal to background ratio for processes (III.9) and (III.10) is possible because there is no direct gluon-gluon induced contribution to $pp \to W^+ t\bar{t}$. However, at some level one must also consider the process

$$pp \to W^+ \, b\bar{t} \, , \qquad (III.13)$$

which is gluon-gluon induced (Fig. 8c), as a background; some fraction of the time the b jet will be misidentified as a t jet. The next section focuses on a thorough calculation of (III.9), (III.10) and (III.13).

IV. Detailed Calculations for

$$pp \to W^+ H, \; pp \to W^+ t\bar{t} \text{ and } pp \to W^+ b\bar{t}$$
$$\hookrightarrow t\bar{t}$$

The Feynmann graphs contributing to

$$pp \to W^+ H \qquad (IV.1)$$
$$\hookrightarrow t\bar{t}$$

$$pp \to W^+ t\bar{t} \qquad (IV.2)$$

$$pp \to W^+ b\bar{t} \qquad (IV.3)$$

are shown in Figs. 8a, 8b and 8c respectively. There is no interference between Feynman diagrams contributing to (IV.1) and those contributing to (IV.2) since such interference terms would correspond to gluon-Higgs mixing proportional to $Tr \, \frac{\lambda^a}{2} = 0$, where a = gluon color index. Process (IV.3) involves a different final state and thus does not have interference terms with (IV.1) or (IV.2).

We have obtained analytic expressions for the invariant matrix elements squared for the reactions (IV.1) and (IV.2). Define the momenta (see Fig. 8a,b,c)

$$\begin{aligned} W - q \\ u(g) - k_1 \\ \bar{d}(g) - k_2 \\ t(b) - p_1 \\ \bar{t} - p_2 \end{aligned} \qquad (IV.4)$$

and invariants as in Eq. II.4 (a-f), with the modification that all the invariants except s_H will be written with carats above them to indicate that they refer to the subprocess. The subprocess matrix element squared (after spin and color averaging) for the reaction (IV.1) is[17]

$$\frac{1}{4N_C^2} \sum_{\substack{\text{spin, color,} \\ \text{helicity}}} |M^{u\bar{d}\to W^+H(\to t\bar{t})}|^2$$

$$= \frac{1}{2}\left(\frac{g_W^3 m_t \cos\theta_c}{2\sqrt{2}}\right)^2 (s_H - 4m_t^2)\, \frac{(\hat{s} + \frac{(m_W^2-\hat{u})(m_W^2-\hat{t})}{m_W^2})}{(\hat{s}-m_W^2)^2}\, \frac{1}{(s_H - m_H^2)^2 + \Gamma_H^2 m_H^2}\,. \qquad (IV.5)$$

Here θ_c is the Cabibbo angle and g_W is the Glashow-Weinberg- Salam $SU(2)_L$ coupling constant. The Higgs width is given approximately by Eq.(II.15). For the physics background (IV.2) of Fig. 8b we obtain the averaged subprocesses matrix element squared[16]

$$\langle |\, M^{u\bar{d}\to W^+ g(\to t\bar{t})}|^2 \,\rangle$$

$$= \frac{2}{9}\left(\frac{g_W g_s^2}{2\sqrt{2}}\right)^2 \frac{1}{s_H^2}\, 8 \left\{ 2\left[\frac{2s_H}{\hat{t}\hat{u}} - m_W^2\left(\frac{1}{\hat{u}^2}+\frac{1}{\hat{t}^2}\right)\right]\right.$$

$$\cdot(\hat{w}^2+\hat{v}^2) + \frac{4m_W^2}{\hat{t}\hat{u}}\,(\hat{w}^2-\hat{v}^2) + 4\hat{w}\hat{v}m_W^2\left(\frac{1}{\hat{t}^2}-\frac{1}{\hat{u}^2}\right) \qquad (IV.6)$$

$$+\frac{4m_t^2+s_H}{2}\left[\frac{\hat{t}}{\hat{u}}+\frac{\hat{u}}{\hat{t}} - m_W^2 s_H\left(\frac{1}{\hat{u}^2}+\frac{1}{\hat{t}^2}\right)\right]$$

$$\left. +\frac{\hat{s}s_H}{\hat{t}\hat{u}}\,(2m_W^2+4m_t^2+s_H)\right\}.$$

For $\langle|\mathrm{M}^{gg\to W^+b\bar{t}}|^2\rangle$ there are eight Feynmann diagrams (Fig. 8c) which, of course, generate many terms. We have not attempted to obtain a simple analytic form for this process. Instead we employed REDUCE to create a subroutine (of considerable length) which evaluates the above $\langle|M|^2\rangle$. We will mention in Appendix A, however, some tricks used to simplify the starting expressions fed into the REDUCE program, and details of the computation. The invariant matrix elements squared were integrated over an appropriate final state phase space and folded together with an appropriate luminosity function ($L_{u\bar{d}}$ for (IV.1) and (IV.2) or L_{gg} for (IV.3)). We employed EHLQ NSET = 2 distribution functions for computing luminosities. We in general imposed a minimum p_T cut on the outgoing W^+, $(p_T)_{min}$. The integral of the $1/t$ poles of Eq. (IV.6), while finite does become large unless such a p_T cut is imposed. In addition we generally imposed rapidity cuts upon the W^+ and "Higgs"/$t\bar{t}$ system. Additional cuts involving the relative orientation of the $t\bar{t}$ system and the overall center of mass system are possible but will not be examined here. We will however consider distributions in the energy of the $t\bar{t}$ quarks.

Our results are presented in Figs. 9 - 14.[18] Process (IV.1) is represented by solid curves in these figures, process (IV.2) by dashed curves and process (IV.3) divided by a factor of 100 by dotted curves. The factor of 10^{-2} used in plotting process (IV.3) can be thought of as a 1/100 b/t jet discrimination ability. In these plots the curves correspond to

$$\int_{m_H^2 - \frac{\Delta m_H^2}{2}}^{m_H^2 + \frac{\Delta m_H^2}{2}} ds_H \, \frac{d\sigma}{ds_H} \equiv \sum(m_H^2) \qquad (IV.7)$$

or various differential distributions of $\sum$, computed for processes (IV.1), (IV.2) or (IV.3). The resolution assumed is

$$\frac{\Delta m_H^2}{m_H^2} = .1 \ . \qquad (IV.8)$$

In view of the discussions of Ref. 19 this may be optimistic. However, it will be apparent from the figure that if such a resolution is achievable and if 1/100 b/t discrimination is possible then a Higgs in the intermediate mass range will be detectable when produced in association with a $W^{\pm}$. The basic cross section for (IV.1), including appropriate cuts, is of order 1 pb, equivalent to 10^4 events in a standard $L = 10^{40}/cm^2$ year. Triggering on the W via its leptonic decays modes into e, μ or τ yields over 1000 events, assuming leptonic detection efficiencies over 50%. If any of the $t's$ or $b's$ decays semi-leptonically, there will be two undetected energetic $\nu's$ in the final state, the first arising from the $W^{\pm}$ decay. We can have at most one undetected energetic ν and still reconstruct accurately the invariant mass of the two-jet system using transverse momentum conservation. Thus, it is necessary to identify the $t's$ and $b's$ only though their purely hadronic modes.

With the numbers given above an efficiency of 40% for t jet identification when the t and, subsequently the b, decay nonleptonically leaves a signal of about 50 events.

Figure 9 shows the cross sections Σ as a function of m_H for $\sqrt{s_L} = 40$ TeV, $-2 < y_W^L,\ y_H^L < 2,\ p_T^W > 40$ GeV. Clearly background (IV.2) is nicely below the signal process (IV.1), while 1 % b/t jet discrimination reduces (IV.3) to a manageable problem.

Figure 10 shows the cross sections as a function of $\sqrt{s_L}$ for $m_H = 130$ GeV, $-2 < y_W^L, y_H^L < 2,\ p_T^W > 40$ GeV. Lower machine energies make the event rate marginal, but do not significantly alter the signal to background ratio. Higher energies increase the b/t discrimination problem.

Figure 11 gives the differential distributions for the top quark energy for $m_H = 130$ GeV, $-2 < y_W^L, y_H^L < 2,\ p_T^W > 40$ GeV, and $\sqrt{s_L} = 40$ TeV. Apparently, cuts in this variable can be used to enhance signal to background somewhat.

Figure 12 gives the differential distributions in p_T^W for $m_H = 130$ GeV, $-2 < y_W^L,\ y_H^L < 2$, and $\sqrt{s_L} = 40$ TeV. From Fig. 12 we see that increasing the minimum allowed value of p_T^W does yield some signal to background enhancement, but only at the sacrifice of event rate.

Figure 13 gives the differential distribution in $\cos\theta_{aco}$, where $\cos\theta_{aco} = (\hat{p}_{beam}^L \times \hat{p}_W^L) \cdot (\hat{p}_{t\ or\ b}^L \times \hat{p}_{\bar{t}}^L)$, for $m_H = 130$ GeV, $-2 < y_W^L,\ y_H^L < 2,\ p_T^W > 40$ GeV, and $\sqrt{s_L} = 40$ TeV. A cut to keep θ_{aco} away from 0° or 180° is desirable.

Figure 14, shows the y_H^L rapidity distribution for $m_H = 130$ GeV, $-2 < y_W^L < 2,\ p_T^W > 40$ GeV. Tightening the rapidity cut enhances signal to background, again at the sacrifice of rate.

Thus the background process (IV.2), of $W + t\bar{t}$ continuum pair produced through an intermediate gluon definitely can be made smaller than the Higgs signal for good resolution in m_H. Top–bottom jet discrimination must be made at the level of $\sim 1\%$, with at least moderate top detection efficiency; in this way the $W^+b\bar{t}$ (or $W^-\bar{b}t$) misidentification background would be adequately suppressed without too great a loss of event rate.

As mentioned earlier satisfactory resolution and b/t discrimination may be difficult to achieve. The study of Ref. 19 which focused on jet pair mass resolution, with specific y_H^L, y_W^L and in particular, p_T^W cuts, is pessimistic in this respect. Given the importance of the intermediate Higgs search we hope that additional cuts and discrimination techniques will be explored in an effort to achieve the required background suppressions. In the event that this does not prove possible it is of paramount importance to search for still other means of seeing the intermediate mass Higgs. Thus, in the next section we explore the signals for Higgs production followed by its decay to a suppressed or "rare" channel, the hope being that the backgrounds could be small.

V. Rare Decay Mode Searches

For $m_H > 2m_t$ but $m_H < 2m_W$ the $t\bar{t}$ mode greatly dominates most other Higgs decay modes. Nonetheless, searches for the Higgs at the SSC in a rare mode are, in many cases, possible in terms of the raw number of events and could have acceptable background levels. In this section we investigate a variety of possibilities of this type.

A. Rare Decay Mode Branching Ratios

We begin by summarizing the branching ratios for Higgs decay into various modes. The modes we consider are:

$$H^0 \to \tau^+\tau^- \quad \text{or} \quad L^+L^- \tag{V.1}$$

$$H^0 \to b\bar{b} \quad \text{or} \quad c\bar{c} \tag{V.2}$$

$$H^0 \to gg \tag{V.3}$$

$$H^0 \to WW^* \tag{V.4}$$

$$H^0 \to ZZ^* \tag{V.5}$$

$$H^0 \to \gamma\gamma \tag{V.6}$$

$$H^0 \to Z\gamma \tag{V.7}$$

$$H^0 \to \Theta\gamma \tag{V.8}$$

In the above L^+L^- refers to some new, heavy lepton pair. The channels are roughly ordered in terms of decreasing branching ratio. We will continue to adopt a t–mass of 40 GeV. All cross sections will be calculated using EHLQ NSET = 2 structure functions for a pp machine at $\sqrt{s} = 40$ TeV.

Most of the partial widths have been calculated analytically in the literature. The familiar fermion pair width formulas applicable to (V.1) and (V.2) are analogous to that in Eq. (II.15). We use the WW^* and ZZ^* results of Ref. 20. The WW^* and ZZ^* partial widths quoted there are obtained when the Z^* or W^* 'decay' channels are summed over. The gg partial width derives from the fermion triangle graphs and has been given in a convenient form in Ref. 20. The $\gamma\gamma$ partial width receives contributions from both fermion and W loops; it has been calculated analytically in Ref. 21. Here, it is a good approximation to ignore all fermions except the t, so long as no new heavy fermions exist.

The $Z\gamma$ width is not directly available in the literature. However, the amplitude for the decay $Z \to H\gamma$ has been given in an approximate form.[22] The width may be written as

$$\Gamma_{H\to Z\gamma} = \frac{1}{32\pi} \frac{(m_H^2 - m_Z^2)^3}{m_H^3} |\mathcal{A}|^2 \qquad (V.9)$$

where $\mathcal{A}$ is the invariant amplitude defined in Ref. 22 as the coefficient of the gauge invariant tensor $(q_\mu k_\nu - k \cdot q g_{\mu\nu})$, where k and q are the γ and Z momenta respectively. In Ref. 22 we find the form

$$\mathcal{A} = \frac{e\, g_W^2 \pi^2}{(2\pi)^4 m_W} (A_F + A_W) \,, \qquad (V.10)$$

where A_F is negligible for light quarks and leptons and is of order .1 for a heavy t quark. We neglect A_F. The dominant contribution is A_W which is well approximated over the range 100 GeV $< m_H <$ 160 GeV by

$$A_W = -4.8 \,. \qquad (V.11)$$

The final mode we consider is (V.8), $H \to \Theta\gamma$. To estimate this we have computed the two continuum graphs for $H \to t\bar{t}\gamma$, and have approximated the invariant amplitude squared, X, near threshold.We find

$$X(m_{t\bar{t}}^2) \approx \frac{4\sqrt{2}\, m_t^2 e_t^2 G_F}{(2\pi)^5} \beta_{t\bar{t}}(m_{t\bar{t}}^2) \qquad (V.12)$$

where $m_{t\bar{t}}$ is the $t\bar{t}$ invariant mass.

We compute the width as

$$\frac{d\Gamma(H \to t\bar{t}\gamma)}{dm^2_{t\bar{t}}} = \frac{\pi^2}{2m_H}\left(1 - \frac{m^2_{t\bar{t}}}{m^2_H}\right)\ X\ (m^2_{t\bar{t}}) \quad . \tag{V.13}$$

We bound the width $\Gamma(H \to \Theta\gamma)$ via the duality integral which sums over all Θ-like states present below continuum threshold:

$$\Gamma(H \to \Theta + \gamma) \simeq \int_{4m_t^2}^{4m_t^2 + \delta 4m_t} dm^2_{t\bar{t}}\ \frac{d\Gamma(H \to t\bar{t}\gamma)}{dm^2_{t\bar{t}}}\ , \tag{V.14}$$

where $\delta = 2m_T - 2m_t$ and m_T is the mass of the first T meson; $\delta \approx 1$ GeV is expected. We find

$$\begin{aligned}\frac{\Gamma(H \to \Theta\gamma)}{\Gamma(H \to t\bar{t})} &\leq \left(\frac{4m_t^2}{m_H^2}\right)\ \frac{16}{27\pi}\alpha_{em}\frac{1}{\beta_{t\bar{t}}(m_H^2)}\left(\frac{\delta}{m_t}\right)^{3/2} + O\left((\frac{\delta}{M_t})^{5/2}\right) \\ &\simeq 6\ \times\ 10^{-6}\ \frac{4m_t^2}{m_H^2}\ \frac{1}{\beta_{t\bar{t}}(m_H^2)}\ .\end{aligned} \tag{V.15}$$

To give an idea of the narrowness of the Higgs and the relative importance of some of the decay modes, we give the partial widths into several channels for $m_H = 130$ GeV. At that mass $\Gamma(H \to t\bar{t}) \approx .19$ GeV, $\Gamma(H \to \tau^+\tau^-) \simeq 2.5 \times 10^{-4}$ GeV, $\Gamma(H \to WW^*) \approx 1.2 \times 10^{-3}\ GeV$, $\Gamma(H \to ZZ^*) \approx 1.1 \times 10^{-4}\ GeV$, $\Gamma(H \to \gamma\gamma) \approx 1.3 \times 10^{-5}$ GeV, and $\Gamma(H \to Z\gamma) \approx .67 \times 10^{-5}$ GeV. The partial width $\Gamma(H \to \Theta\gamma)$ is at least a factor of 10 smaller than those of the $\gamma\gamma$ and $Z\gamma$ modes at $m_H = 130$ GeV.

All of the above branching ratios for the decay modes (V.1)-(V-8) are plotted as a function of m_H in Fig. 15. These results will allow us to assess the feasibility of observing the Higgs in any of the rare decay modes.

B. Inclusive Higgs Production followed by Rare Decay

We first focus on inclusive (i.e. nonassociative) production of a single Higgs followed by its decay into one of the rare channels. The cross sections for single Higgs production are tabulated in the EHLQ supplement,[10] for $pp \to H^0 \to t\bar{t}$ with $|y_{t,\bar{t}}| < 1.5$. We will compute our signal for the two body decay channels, (V.1)-(V.3) and (V.6)-(V.8), as follows. We write

$$\begin{aligned} \Sigma_{SIG}(ab) &\equiv \sigma(pp \to H \to ab)|_{|y_{a,b}|<1.5} \\ &= \sigma(pp \to H \to t\bar{t})|_{|y_{t,\bar{t}}|<1.5} \cdot \frac{\Gamma(H \to ab)}{\Gamma(H \to t\bar{t})} \kappa_{ab} \ . \end{aligned} \tag{V.16}$$

In Eq. (V.16) κ_{ab} is a correction factor that takes into account effects of the masses of a and b relative to m_t. Due to the different dependence on m_a and m_b in the phase space component of $\Gamma(H \to ab)$ compared to the inclusive integral on which we impose the rapidity cut $|y_{a,b}| \leq 1.5$, κ will in general not be precisely 1. However, in all cases it is quite near unity since the rapidity distributions of a, b are very similar to those of the t and $\bar{t}$ at small y. The factorized form exhibited in Eq. (V.16) only holds because the Higgs is a scalar, implying that $\frac{d\sigma}{d\hat{t}}$ is independent of $\hat{t}$ and $\hat{u}$. For the two-body modes (V.1-V.3 and V.6-V.8) the background is computed generally as

$$\Sigma_{BG}(ab) = \Delta m_{ab} \left. \frac{d\sigma(pp \to ab)}{dm_{ab}} \right|_{|y_{a,b}| < 1.5 \text{ and } m_{ab} = m_H} , \tag{V.17}$$

where $\Delta m_{ab} = f_{ab}\, m_H$ and f_{ab} depends on the particular channel.

V.1 LEPTON PAIR MODES

For the lepton pair channel (IV.1) we will consider both $H \to \tau^+\tau^-$ and $H \to L^+L^-$ where L is a heavy lepton with $m_L > m_\tau$. Even though some aspects of the process $H \to \tau^+\tau^-$ have been considered in Ref. 23, we find it useful to review the situation here. Of course, only m_L values above current experimental limits but below m_W are of interest. The irreducible background comes from lepton pair production through an intermediate virtual γ or Z. We have computed the Drell-Yan background arising from $q\bar{q}$ annihilation including the same rapidity cuts as for the signal (see Eqs. V.16 and V.17). The irreducible background receives an additional contribution which could be of roughly the same size arising from the process of gluon-gluon fusion into a lepton pair through a quark loop and virtual Z or γ. The extra factor of α_s^2 could be compensated by the large gg luminosity. In fact, the calculations of Ref. 24 indicate that in the absence of a new heavy quark with mass greater than .2 TeV the normal Drell-Yan background will dominate.

We present our results for $H \to \tau^+\tau^-$ in Fig. 16. The mass resolution used was

$$\Delta m_{\tau^+\tau^-} = .05\ m_H\ . \qquad (V.18)$$

This is certainly optimistic due to the loss of neutrinos in the τ decay. We find that typically (see Eqs. (V.16) and (V.17))

$$\frac{\Sigma_{SIG}(\tau^+\tau^-)}{\Sigma_{BG}(\tau^+\tau^-)} \sim .2\ . \qquad (V.19)$$

In addition, there are other, reducible backgrounds to contend with in practice.

The first which we will mention arises from the process

$$pp \rightarrow \underset{\hookrightarrow \tau + \ldots}{Q} \quad + \quad \underset{\hookrightarrow \tau + \ldots}{\overline{Q} + X} \quad , \tag{V.20}$$

where the additional particles in the fragmentation of Q, a heavy quark, are lost due to detector cuts. We have not attempted to estimate this background. However, it could be large because $Q\bar{Q}$ production can proceed as a gluon-gluon initiated process.

A second problem emerges when one considers that the reconstruction in $m_{\tau^+\tau^-}$, the invariant mass of the τ-pair, will be poor. Some of the time the reconstructed mass will fall below m_Z. Such an event can be produced far more readily through the production of an on-shell Z followed by its decay into $\tau^+\tau^-$. Effectively, then, only the portion of the reconstructed $m_{\tau^+\tau^-} \geq m_Z$ can be used in the signal identification.

Finally, the $\tau's$ must be identified in some way. The manner in which this is done can result in the presence of other backgrounds. As an example, one could try to identify a τ in its decay modes of $\pi\nu$ or $\rho\nu$, $[BR(\tau \rightarrow \pi\nu \text{ or } \rho\nu) \approx .32]$, channels which have the minimal number of charged tracks and lost neutrinos. Two isolated hadrons, though, can arise through the fragmentation of two quarks or gluons, each into a single fast π or ρ and other slow particles which cannot be assigned to either jet reliably. Crude estimates suggest that this would be a severe problem. Such additional backgrounds could be significantly reduced by employing a vertex detector to observe the decay of the τ. Whether or not it is possible for a vertex detector to function in this role at an instantaneous luminosity of $10^{33}/cm^2sec$ is an open question worthy of study.

The signal cross section varies over the range considered from .04 pb to .4 pb, implying a few thousand events for integrated luminosity of $L = 10^{40}/cm^2$. Ignoring the reducible backgrounds the raw number of events in the signal appears to be sufficient for the enhancement shown in Eq. (V.19) to be observable provided the shape of the background is smooth relative to the signal. However, the experimental mass resolution, expected to be substantially worse than that of Eq. (V.18), would obscure any peaking of the signal. Then, a prediction for the absolute event rate of the background would be necessary in order to detect a spread out enhancement. Because of K factors, distribution function uncertainties, etc., the background is uncertain in normalization by $\sim 20\%$. We are rather pessimistic, therefore, concerning the prospects of observing the Higgs in the $\tau^+\tau^-$ channel even without consideration of the reducible backgrounds.

Many of the same considerations apply to the case of a heavy lepton pair. The advantage of a heavier lepton is, of course, the increased branching ratio for $H \to L^+L^-$ (if m_L is not too close to $m_H/2$). We present in Fig. 17 the curves for the signal and irreducible background, arising through the Drell-Yan mechanism as a function of m_L for a selection of Higgs masses. We arbitrarily begin our plots at $m_L = 10$ GeV. Retaining the mass resolution of Eq. (V.18), it is apparent that

$$\left(\frac{\Sigma_{SIG}(L^+L^-)}{\Sigma_{BG}(L^+L^-)}\right) \geq 1 \qquad m_L > 15 \text{ GeV} \qquad (V.21)$$

In fact the ratio is substantially greater than 1 for the higher values of m_L. Only if m_H is near the Z mass does the irreducible background begin to present a problem.

As for the $\tau^+\tau^-$ case the process $gg \to$ quark loop $\to Z^*$ or $\gamma^* \to L^+L^-$

contributes negligibly to the background unless there is a new heavy quark (with mass greater than $\approx .2$ TeV) contributing to the amplitude. Thus, although the mass resolution assumed is probably quite optimistic, the irreducible background does not appear to be large enough to allow us to dismiss the heavy lepton pair signature as impractical.

The significance of the reducible background is less certain. Assuming that we look for L in a hadronic decay mode and that the lifetime of L is too short for vertex detection the most serious background is likely to be from the two jet processes in which each jet mimics the heavy L mode being utilized. Since leptons heavier than the τ will decay more frequently into modes which involve several hadrons, this problem could be severe depending upon how rapidly the $H \rightarrow L^+L^-$ branching ratio grows with increasing m_L in comparison to how rapidly the importance of multiparticle decay modes increases. Independent of vertex detection and the mode of L identification, there are also the $Z \rightarrow L^+L^-$ and $Q\bar{Q} \rightarrow L^+L^-$ + (lost or missing) backgrounds to be considered. Nonetheless, if a heavy lepton exists this possible mode of Higgs discovery deserves further study.

V.2 $b\bar{b}$, $c\bar{c}$, AND gg MODES

The $b\bar{b}$ and $c\bar{c}$ decay modes (V.2) are certainly unusable. We have already seen in Sec. III that (assuming a 5% mass resolution in a hadronic channel) H is unobservable in its primary $t\bar{t}$ decay mode due to backgrounds from QCD $t\bar{t}$ production. The background $b\bar{b}$, $c\bar{c}$ cross sections will be the same order as for $t\bar{t}$ whereas the signal cross section is substantially reduced due to the small branching ratio for $H \rightarrow b\bar{b}$, $c\bar{c}$ decay, see Fig. 15, which are of order .07 to .02

for $b\bar{b}$ and .006 to .002 for $c\bar{c}$.

These same remarks apply also to the gg decay mode (V.3). The gg branching ratio varies from .02 to .007 while the QCD background gg cross section is even larger than the above $q\bar{q}$ cross sections.

V.3 $\gamma\gamma$ AND γZ MODES

We next focus on the $\gamma\gamma$ and γZ modes (V.6) and (V.7). The Z will almost certainly be found in its e^+e^- or $\mu^+\mu^-$ channel in which case the invariant mass resolution will be considerably better than Eq. (V.18). We take

$$(\Delta m)_{\gamma\gamma} = (\Delta m)_{Z\gamma} = .01 m_H \quad . \tag{V.22}$$

We plot in Fig. 18 the background and signal cross sections Σ_{BG} and Σ_{SIG}, defined by Eqs. (V.16) and (V.17). The backgrounds were computed at tree graph level using $q\bar{q}$ collisions. (There is a possibly significant background arising from $gg \to Z\gamma$ or $\gamma\gamma$ using a fermion loop mechanism; the extra α_s^2 can be compensated by the larger gluon luminosity.) We find

$$\frac{\Sigma_{SIG}(Z\gamma)}{\Sigma_{BG}(Z\gamma)} \leq \frac{1}{20}\,, \tag{V.23}$$

while

$$\frac{\Sigma_{SIG}(\gamma\gamma)}{\Sigma_{BG}(\gamma\gamma)} \leq \frac{1}{10}\,. \tag{V.24}$$

Though these are not absurdly small ratios the associated event rates are very marginal. Not including the Z branching ratio to lepton pairs we have at $m_H =$

130 GeV for instance

$$L\Sigma_{SIG}(\gamma\gamma) \approx L\Sigma_{SIG}(Z\gamma) \;=\; 60 \text{ events} \qquad (V.25)$$

compared to (also at $m_H = 130$ GeV)

$$\begin{aligned} L\Sigma_{BG}(\gamma\gamma) &= 1000 \text{ events} \\ L\Sigma_{BG}(Z\gamma) &= 8000 \text{ events} \end{aligned} \qquad (V.26)$$

for $L = 10^{40}/cm^2$. Since the $\gamma\gamma$ channel has no additional branching factor to be included and also $\gamma\gamma$ has the larger Σ_{SIG}/Σ_{BG} values it is the preferred mode. However, a 60 event excess in 1000 events is only a 2σ effect.

V.4 $\Theta\gamma$ Mode

The final two body mode we have considered is $H \rightarrow \Theta\gamma$, (V.8) where we imagine detecting the Θ in its e^+e^- or $\mu^+\mu^-$ decay modes for which the best mass resolution is achievable without significant Θ branching ratio sacrifices. We have used the procedure described earlier to compute the required $H \rightarrow \Theta\gamma$ branching ratio. At $m_H = 130$ GeV the branching ratio is $\lesssim 3 \times 10^{-6}$.

The corresponding event rate at $m_H = 130$ GeV is

$$L\Sigma_{SIG}(\Theta\gamma) \leq 3 \text{ events} . \qquad (V.27)$$

Because of the useless event rate we have not estimated backgrounds.

V.5 WW^* AND ZZ^* MODES

We now turn to the WW^* and ZZ^* decay modes of the Higgs, (V.4) and (V.5). The signal cross section is computed approximately as (for example)

$$\tilde{\Sigma}_{SIG}(WW^*) = \Sigma_{SIG}(t\bar{t}) \frac{\Gamma\left(H \to WW^*(\to \bar{f}f')\right)}{\Gamma(H \to t\bar{t})} \qquad (V.28)$$
$$\hookrightarrow \bar{f}f'$$

which neglects the κ correction factor of Eq. (V.16). The cross sections as functions of m_H are plotted in Fig. 19, where all light fermion modes are summed over. (Light fermion modes for the W^{+*} include $(u\bar{d})$, $(c\bar{s})$, $e^+\nu$, $\mu^+\nu$, $\tau^+\nu$ for $m_H < 135$ GeV, with the addition of $(t\bar{b})$ for $m_H > 135$ GeV; for the Z^* only the $t\bar{t}$ and $\nu\bar{\nu}$ modes are excluded.) In addition W^+W^{-*} and W^-W^{+*} are summed. We see that

$$\frac{\tilde{\Sigma}_{SIG}(WW^*)}{\tilde{\Sigma}_{SIG}(ZZ^*)} = \begin{cases} 300 & m_H = 100 \text{ GeV} \\ 15 & m_H = 160 \text{ GeV} \end{cases}, \qquad (V.29)$$

and that

$$L\tilde{\Sigma}_{SIG}(WW^*) = \begin{cases} 300 \text{ events} & m_H = 100 \text{ GeV} \\ 4 \times 10^4 \text{ events} & m_H = 160 \text{ GeV} . \end{cases} \qquad (V.30)$$

There are a variety of channels in which to search for a WW^* or ZZ^* signal. The best mass resolution is achieved in the ZZ^* mode in which both the Z and Z^* are detected in lepton pair modes. This latter restriction reduces the event rate by a factor of about

$$\left(\Gamma(Z \to \mu^+\mu^-, e^+e^-)/\Gamma_Z^{Tot}\right)^2 = 3.6 \times 10^{-3} \qquad (V.31)$$

yielding at $m_H = 160$ GeV only 10 events. In the other extreme, we could require that both the W and W^* or Z and Z^* decay to hadronic jets. The QCD

4-jet background would, however, be overwhelming. Then, it is most useful to consider the configuration in which the $W(Z)$ decays into two hadronic jets while the $W^*(Z^*)$ decays leptonically. The backgrounds to the reverse situation in which $W^*(Z^*)$ decays hadronically while $W(Z)$ decays leptonically will be larger since the $W^*(Z^*)$ hadronic decay can be more easily mimiced by a virtual gluon decay than the on-pole $W(Z)$ hadronic decay. An exception to this observation occurs when $m_H - m_W$ is of order m_W. Then the peaking in m_{W^*} as m_{W^*} approaches m_W can be used to approximately solve for the momentum of the ν (assuming the momenta of the charged lepton and quark jets are measured), and thus reconstruct m_H. For convenience, in our discussion of backgrounds we will restrict our attention to the WW^* case since its event rate is larger than the ZZ^*mode.

There are a variety of possible backgrounds to the preferred configuration:

$$pp \to H \to W(\to q_1\bar{q}_2)W^*(\to \ell\bar{\nu}_e) \quad . \tag{V.32}$$

The irreducible background yielding an identical final state arises from the continuum production process:

$$pp \to W(\to q_1\bar{q}_2)W^*(\to e\bar{\nu}_e) \quad . \tag{V.33}$$

We have evaluated the cross section for this process in a very crude approximation in which the only m_{W^*} variation appears in the W^* propagator. We find (before including any $W \to q_1\bar{q}_2$ branching ratio)

$$\begin{aligned} &\Sigma_{BG}(WW^*) \leq 10^{-3} \text{ pb} \\ &\qquad\quad \llcorner\!\!\to e\bar{\nu}_e \end{aligned} \tag{V.34}$$

at $m_H = 130$ GeV, assuming a mass resolution of

$$\Delta m_{WW^*} = .05\, m_H \ . \qquad (V.35)$$

In order to compare Eq. (V.34) to the signal cross section of Fig. 19, the signal should be divided by a factor of $\frac{1}{9}$ corresponding to a single $f\bar{f}'$ mode (+ charge conjugate). This yields at $m_H = 130$ GeV

$$\tilde{\Sigma}_{SIG}(WW^*) = 7 \times 10^{-2} \text{ pb} \quad . \qquad (V.36)$$
$$\hookrightarrow \ell\bar{\nu}_\ell$$

Clearly, unless the effects of off-shell m_{W^*} dependence in the matrix elements are dramatic, the irreducible background should not be significant under the assumption of the resolution of Eq. (V.35).

However, Eq. (V.35) is far too optimistic since the ν-four momentum cannot be determined solely from transverse momentum conservation when the invariant mass of the charged lepton and neutrino is variable. It is even possible for the invariant mass of the neutrino and charged lepton to be m_W, yet the observed kinematics to be consistent with the interpretation of the event as arising from the signal. Although the constraints on the phase space of the on-shell W decay are severe in order that the decay of the two $W's$ mimic the signal, the enhancement obtained by putting the intermediate W on-shell is quite significant. Therefore, it is necessary not only to degrade the resolution of Δm_{WW^*} in Eq. (35), but also to include with the appropriate cuts the background

$$pp \to H \to WW \qquad (V.37)$$
$$\hookrightarrow \ell\bar{\nu}_\ell \quad .$$

A careful assessment of these backgrounds will be left to a later work.

Finally, we briefly consider the background

$$pp \to q_1\bar{q}_2(W^* \text{ or } W) \qquad (V.38)$$

which occurs via the graph of Fig. 20 - this process makes full use of the gluon luminosity. It is a background due to the fact that we imagine triggering on the W in a $q_1\bar{q}_2$ mode so that reconstruction of the Higgs mass might be possible. This is closely analogous to the problem of reconstructing a single inclusively produced W in a hadronic decay channel, despite the presence of $q_1\bar{q}_2$ continuum; without determining the jet charge the same gluon luminosity appears in the latter background calculation.

There is a quite similar problem to be faced when $m_H > 2m_W$. The signature of $H \to WW \to 2$ jets $+ \ell\nu$ faces a mixed QCD and electroweak background from continuum 2 jet + W production. The background is quite troublesome for $m_H > 2m_W$, [25] and it will be worse for $m_H < 2m_W$.

In summary the only potentially viable modes in the search for a rare decay of an inclusively produced Higgs appear to be a possible heavy lepton L^+L^- mode and the $W(\to q_1\bar{q}_2)\ W^*(\to \ell\bar{\nu}_\ell)$ or $Z(\to q\bar{q})\ Z^*(\to e^+e^-)$ modes. Both have backgrounds that require further investigation.

C. Associated Higgs Production Followed by Rare Decay

In a continuing effort to find a truly identifiable signature, we turn to associated production of the Higgs followed by its decay into one of the rare modes. We shall discuss the production of

$$t\bar{t} + H^0\ , \qquad (V.39)$$

$$W^{\pm} + H^0 \ , \tag{V.40}$$

$$Z + H^0 \ , \tag{V.41}$$

followed by $H^0 \to WW^*$, ZZ^* or $\tau^+\tau^-$.

It is convenient to begin with the $W^{\pm}+H^0$ and $Z+H$ modes with $H^0 \to WW^*$ or ZZ^* decay. We demand that the final state contain at most one energetic neutrino; this allows (partial) reconstruction of both the ($W^{\pm}$ or Z) and H mass, and a consequent reduction in background. Such reconstruction is only likely to be possible if, in addition, we require that no b or t jets are present. Finally, we demand that W^* or Z^* appear in an "e" or "μ" leptonic mode since this considerably reduces combinatoric jet backgrounds and eliminate many gg collision backgrounds. Of course as discussed earlier, this also implies, in the case $H \to WW^*$, that the associated neutrino's four-momentum cannot be fully reconstructed since its source is an off-shell W^* of variable mass. The resulting loss of mass resolution in the m_{WW^*} variable is considerable. The alternative in which $H \to WW^*$ with $W \to \ell\nu_\ell$ and $W^* \to q_1\bar{q}_2$ allows for reconstruction of the neutrino four-momentum. However, the background would be far larger than in the previous configuration because no mass cut in the hadronic $q_1\bar{q}_2$ channel is then possible. Let us define the following sets of states.

$$S_1 = \left\{u\bar{u},\ d\bar{d},\ c\bar{c},\ s\bar{s}\right\} \tag{V.42}$$

$$S_2 = \left\{e^+e^-,\ \mu^+\mu^-\right\} \tag{V.43}$$

$$S_3 = \left\{u\bar{d},\ c\bar{s}\right\} \tag{V.44}$$

$$S_4 = \left\{e^+\nu_e,\ \mu^+\nu_\mu\right\} \tag{V.45}$$

We then sum over the following processes:

$$pp \to Z(\to S_1 \ + \ S_2) \ + \ H\,(\to Z(\to S_1 + S_2) \ + \ Z^*(\to S_2)) \ , \qquad (V.46)$$

$$pp \to \ Z(\to S_1 + S_2) \ + \ H\,(\to W^{\pm}(\to S_3 \text{ or } \bar{S}_3) + W^{\mp *}(\to \bar{S}_4 \text{ or } S_4)) \ , \ (V.47)$$

$$pp \to \ W^{\pm}(\to S_3(\text{ or } \bar{S}_3) + S_4(\text{ or } \bar{S}_4)) + H(\to Z(\to S_1 + S_2) + Z^*(\to S_2)) \ , \ (V.48)$$

$$pp \to \ W^{\pm}(\to S_3 \text{ or } \bar{S}_3) + H(\to W^{\pm}(\to S_3 \text{ or } \bar{S}_3) + W^{\mp *}(\to \bar{S}_4 \text{ or } S_4)) \ . \ (V.49)$$

We use the approximate cross sections[10] at $\sqrt{s} = 40\ TeV$ for $pp \to Z + H$ and $pp \to W^{\pm} + H$ as listed in Table V.A.

Table V.A

m_H	110	135	160	(GeV)
$\sigma(pp \to Z + H)$	4 pb	3 pb	2 pb	
$\sigma(pp \to W^{\pm} + H)$	7 pb	5.5 pb	4 pb	

The gg initiated process, $gg \to$ fermion loop $\to Z + H^0$, which would enhance the $Z + H$ cross section has not been included.

Folding in the branching ratio for Higgs decay into ZZ^* or $W^{\pm}W^{\mp *}$ as given in Fig. 15, along with the branching ratios of the gauge bosons into the channels specified in (V.47)–(V.50), we obtain

$$\Sigma(pp \to (W^{\pm} \text{ or } Z)H)\times \text{(Effective Branching Ratio)} = \begin{cases} 3.5\ 10^{-4} \text{ pb} & m_H = 110 \text{ GeV} \\ 4.0\ 10^{-3} \text{ pb} & m_H = 135 \text{ GeV} \\ 2.5\ 10^{-2} \text{ pb} & m_H = 160 \text{ GeV} \ . \end{cases} \qquad (V.50)$$

The effective cross sections of Eq. (V.51) correspond, at $L = 10^{40}/cm^2$, to 3.5, 40, and 250 events respectively. Apparently, above $m_H = 135$ GeV the raw

event rate becomes significant, and it is worth considering backgrounds to the decay modes. Details of this topic will be left to a future paper. We confine ourselves here to outlining possible backgrounds.

Consider, for example, process (V.47). Examples of backgrounds are illustrated in Fig. 21. In Fig. 21a we find a process that is a background when both $Z's$ decay into S_1 type states; Fig. 21b and c are backgrounds to events of type (V.47) when at least one Z decays into S_1, type states. Finally, Fig. 21d is an irreducible background to all processes in (V.53) which, unlike mechanisms a - c cannot be reduced by improving mass resolution in the on-shell Z channels. Clearly, computation of these backgrounds will be an arduous task. The other modes (V.48)–(V.50) have entirely similar types of backgrounds.

Next, we briefly consider the $t\bar{t} + H$ production

$$\begin{array}{l} pp \rightarrow t\bar{t}+H \\ \qquad\qquad \hookrightarrow ZZ^* \text{ or } WW^* \ . \end{array} \qquad (V.51)$$

The $t\bar{t}$ channel, of course, is not resonance dominated, and a wide spectrum of $t\bar{t}$ masses is relevant. In addition, $t\bar{t}$ decay will be associated with a significant number of unobserved neutrinos. If the H decays to WW^* and either the W or W^* decays leptonically then the additional neutrino will make the H^0 mass difficult to reconstruct. If both W and W^* decay hadronically there will be large QCD $t\bar{t}$ + 4 jet backgrounds.

Therefore, the $H \rightarrow ZZ^*$ decay mode appears to be the more feasible. However, the decay of $H \rightarrow ZZ^*$ followed by a reconstructable decay $Z \rightarrow S_1 + S_2$, $Z^* \rightarrow S_2$ (the S_2 restriction on the Z^* decay eliminates $t\bar{t}$ + 4 jet backgrounds)

yields a net branching ratio of

$$\text{Effective Branching Ratio} = \begin{cases} 8.3\ 10^{-7} & m_H = 110\ \text{GeV} \\ 3.8\ 10^{-5} & m_H = 135\ \text{GeV} \\ 2.5\ 10^{-4} & m_H = 160\ \text{GeV} \end{cases} . \qquad (V.52)$$

The cross section for $t\bar{t} + H$ is ≤ 20 pb[16] without any cuts on t, $\bar{t}$ or H momenta. This cross section corresponds to 2×10^5 events at $L = 10^{40}/cm^2$. Only at $m_H = 160$ is a significant number of events in the above ZZ^* decay modes (≈ 50) predicted. There are, however, many possible backgrounds; these backgrounds cannot be reduced by improved mass resolution in the $t\bar{t}$ channel which was not resonance dominated to begin with. Thus, we are not optimistic regarding this process as a possible Higgs search mode.

Next consider[23]

$$\begin{array}{l} pp \rightarrow W^{\pm}\ ,\ Z + H \\ \qquad\qquad\quad \llcorner\!\!\rightarrow \tau^+\tau^- \end{array} \qquad (V.53)$$

In this reaction neutrinos inevitably inhibit a direct reconstruction of the H mass using the decay products of the $\tau's$. However, if the $W^{\pm}$ or Z transverse momentum, p_T, is known then the H mass may be reconstructed provided the τ decay jets are not collinear in the transverse momentum plane. Write[26]

$$p_\tau \rightarrow p_o + p_{\text{miss}} \qquad (V.54)$$

corresponding to

$$\tau \rightarrow (\text{observed}) + (\text{missing}) . \qquad (V.55)$$

By noting that to a good approximation $\vec{p}_o \parallel \vec{p}_{miss}$, we may write

$$\frac{|\vec{p}_{miss}|}{|\vec{p}_\tau|} = x, \quad \frac{|\vec{p}_o|}{|\vec{p}_\tau|} = (1-x) , \qquad (V.56)$$

and obtain (T = transverse)

$$\begin{aligned}(\vec{p}^T) &= \vec{p}^T_{\tau_1} + \vec{p}^T_{\tau_2} \\ &= \frac{\vec{p}^T_{o_1}}{(1-x_1)} + \frac{\vec{p}^T_{o_2}}{(1-x_2)} \,.\end{aligned} \tag{V.57}$$

Eq. (V.58) yields two simultaneous equations to be solved for x_1 and x_2. Given x_1 and x_2 we compute

$$\begin{aligned}m_H^2 = (p_{\tau_1} + p_{\tau_2})^2 &\approx 2p_{\tau_1} \cdot p_{\tau_2} \\ &= \frac{1}{(1-x_1)} \frac{1}{(1-x_2)} 2p_{o_1} \cdot p_{o_2} \quad .\end{aligned} \tag{V.58}$$

It is highly desireable in (V.54) to use the decays $Z \to S_1$ or S_2, or $W^\pm \to S_3(\bar{S}_3)$, since in the decay $W^\pm \to S_4(\bar{S}_4)$ it is not possible to directly measure the p_T of the W, and so by the previous discussion fix m_H. Without reconstruction of m_H the processes

$$\begin{aligned} &pp \to (W^\pm,\ Z) + Z\ +\ X, \quad pp \to (W^\pm, Z) + Q\bar{Q} + X \\ &\qquad\qquad \big\lfloor\!\!\to \tau^+\tau^- \end{aligned} \tag{V.59}$$

become troublesome backgrounds. (See the discussion given earlier for inclusive production of $H \to \tau^+\tau^-$ in the presence of the backgrounds $Z \to \tau^+\tau^-$ and $Q\bar{Q} \to \tau^+\tau^-$ + (lost or missing).) We then choose not to include the $S_4(\bar{S}_4)$ modes in the following analysis. Including the branching ratios for $Z \to S_1$ or S_2 or $W^\pm \to S_3(or\bar{S}_3)$ and for $H \to \tau^+\tau^-$ as given in Fig. 15, and using the cross sections of Table V.A, we obtain

$$\sigma\left(pp \to\ Z(\to S_1 \text{ or } S_2)\ +\ H(\to \tau^+\tau^-)\right) = \begin{cases} 7.2 \times 10^{-3}\text{pb} & m_H = 110 \text{ GeV} \\ 1.2 \times 10^{-3}\text{pb} & m_H = 160 \text{ GeV} \end{cases}$$

$$\sigma\left(pp \to W^{\pm}(\to S_3) \ + \ H(\to \tau^+\tau^-)\right) \ = \ \begin{cases} 1 \times 10^{-2}\text{pb} & m_H \ = 110 \text{ GeV} \\ 1 \times 10^{-3}\text{pb} & m_H \ = 160 \text{ GeV} \end{cases} . \tag{V.60}$$

As discussed previously, if the Higgs $\vec{p}_T$ can be reconstructed it is not necessary to restrict the τ decay modes. However, the presence of $\tau's$ must be an integrated part of the trigger in order to avoid backgrounds arising from $pp \to (W^{\pm},\ Z) + 2$ jets etc., when the 2 jets each are composed of low multiplicity fragments. Such events could mimic the $(W^{\pm},\ Z) \ + \ \tau^+\tau^-$ final state. The ideal solution is to have a vertex detector which would eliminate this background without significantly restricting the τ decay modes. At $\mathcal{L} = 10^{33}/cm^2$ /sec $(L = 10^{40}/cm^2)$, Eq. (V.61) implies ≈ 200 events in the

$$\begin{array}{l} (W^{\pm}, Z)H \\ \qquad \big\lfloor\!\!\rightarrow \tau^+\tau^- \end{array} \tag{V.61}$$

mode at $m_H = 160$ GeV. If vertex detectors can only operate at $\mathcal{L} = 10^{32}/cm^2/$ sec then these rates become more marginal.

Finally, we consider

$$\begin{array}{l} pp \to t\bar{t}+H \\ \qquad\quad \big\lfloor\!\!\rightarrow \tau^+\tau^- \end{array} \tag{V.62}$$

Note that the t and $\bar{t}$ decays often lead to the presence of energetic neutrinos. It will be more difficult to determine p_T^H in (V.63) than in the previous process, and so m_H will be more poorly measured. As the cross sections for the two reactions are nearly the same, there appears to be no advantage in pursuing (V.62) over (V.54).

This survey of associated Higgs production suggests that the modes (V.47)-(V.50) involving associated production of H and $W^{\pm}$ or Z followed by appro-

priate WW^* or ZZ^* decays of H could possibly allow for an intermediate mass Higgs search in the range 135 GeV $< m_H <$ 160 GeV. The process ($W(\rightarrow S_3$ or $\bar{S}_3)$, $Z(\rightarrow S_1$ and $S_2)) + H^0(\rightarrow \tau^+\tau^-)$ could be of use throughout the range 100 GeV $< m_H <$ 160 GeV. Assuming for the moment that vertex detectors can operate at $L = 10^{40}/cm^2$ the $H \rightarrow \tau\tau$ decay modes have a distinct advantage over the $H \rightarrow WW^*$ case of the first mode because m_H can be reconstructed in full as described in Eqs. (V.55) – (V.59). Arduous background calculations are required to further assess these possibilities.

VI. CONCLUSION

In conclusion we have examined various means for detecting an intermediate mass Higgs, $2m_t < m_H < 2\ m_W$. It is clear from our discussions that e^+e^- collisions are far superior for such a search due to the lack of significant backgrounds (except for Higgs with weaker couplings than in the standard model) in modes such as $e^+e^- \rightarrow ZH$. In our survey of pp collisions only a very few search modes proved even marginally feasible. These include:

(a) $pp \rightarrow WH(\rightarrow t\bar{t})$. Physics backgrounds are manageable and event rates significant, but required detector mass resolution in m_H and $t - b$ jet discrimination may be difficult to achieve.

(b) $pp \rightarrow H(\rightarrow L^+L^-)$ with L being a heavy lepton–QCD two jet events with jet decay to states that mimic the various L decay modes could be a problem even for the otherwise favorable $m_L \geq 15$ GeV range.

(c)

$$pp \rightarrow H \begin{cases} \rightarrow WW^* \\ \rightarrow ZZ^* \end{cases}$$

with W^*, Z^* decay to a leptonic mode and W, Z detection in a fully reconstructable mode. However, in the situation where $H \to WW^*$ the resolution in the H mass is comparatively poor. A variety of background calculations are required to further evaluate this possibility.

(d)

$$pp \to (W^{\pm}, Z) + H$$
$$\qquad\qquad\qquad\qquad\qquad\qquad \llcorner\!\!\to \begin{matrix} WW^* \\ ZZ^* \end{matrix}$$

with W^*, Z^* decay to a leptonic mode and W, Z decay reconstructable. Again, in the situation where $H \to WW^*$ the resolution in the H mass is comparatively poor, and nontrivial background calculations are required.

(e)

$$pp \to (W^{\pm},\ Z) + H$$
$$\qquad\qquad\qquad\qquad\qquad\qquad \llcorner\!\!\to \tau^+\tau^-$$

with W and Z decays fully reconstructable. This signature would benefit if it were possible to use vertex detectors at full luminosity. It has the advantage over (c) and (d) that the H mass may always be fully determined. However, additional background calculations are required. Relative to this mode the process $pp \to t\bar{t} + H(\to \tau^+\tau^-)$ is much less attractive due to the inability to directly reconstruct the H transverse momentum and hence mass.

We summarize in Table VI.A the processes considered, backgrounds computed and backgrounds worthy of further study.

Of course, the best procedure would be to design machines which overcome the problem referred to above. Two obvious possibilities emerge. The first is to give increased consideration to higher energy e^+e^- machines based on emerging

technology. The second is to design the SSC so that a high luminosity interaction region with $\mathcal{L} \simeq 10^{35}/\mathrm{cm}^2/\mathrm{sec}$ could be incorporated. Such a luminosity makes the comparatively background free modes

$$pp \to H \begin{cases} \hookrightarrow Z \begin{cases} \hookrightarrow e^+e^- \text{ or } \mu^+\mu^- \end{cases} \\ Z* \begin{cases} \hookrightarrow e^+e^- \text{ or } \mu^+\mu^- \end{cases} \end{cases}$$

and perhaps

$$pp \to Z \begin{cases} \hookrightarrow e^+e^- \text{ or } \mu^+\mu^- \end{cases} \qquad H \begin{cases} \hookrightarrow \tau^+\tau^- \end{cases}$$

viable on an event rate basis. For this interaction region only a veto against accompanying hadrons need be incorporated in order to eliminate heavy-quark backgrounds.

ACKNOWLEDGEMENTS

We acknowledge K. Lane as a contributor to the results of Section IV. We thank W. Bardeen, M. Chanowitz, L. Clavelli, F. Halzen, and F. Paige for useful suggestions. We thank Z. Kunszt for correspondences regarding the work of Section IV.

Table VI.A

Mode	Backgrounds Computed	Worthy of further study?; Calculations to be done.
(Inclusive)		
$H \to t\bar{t}$	$pp \to t\bar{t} + X$	No
$H \to \tau^+\tau^-$	Drell-Yan $pp \to \tau^+\tau^- + X$	Perhaps; resolution in $\tau^+\tau^-$ invariant mass
$H \to L^+L^-$	Drell-Yan $pp \to L^+L^- + X$	Yes; $Q\bar{Q} \to L^+L^-$ + (lost) background, mass resolution and signature studies
$H \to \gamma\gamma$	$pp \to \gamma\gamma + X$	No
$H \to Z\gamma$	$pp \to Z\gamma + X$	No
$H \to \Theta\gamma$	–	No
$H \to W\bar{f}f'$	$pp \to WW^*(\to \bar{f}f')$ + X estimated	Yes; signal calculation with rapidity cuts included properly, backgrounds of e.g. $W^+\bar{e}\nu_e$, 2 jets + $e^-\nu_e$. Effects of having only H transverse mass reconstruction
$H \to Z\bar{f}f$	$pp \to ZZ^*(\to \bar{f}f)$ + X	Analogous comments to $H \to W\bar{f}f'$, except no problem with reconstructing H mass.
(Associated)		
$t\bar{t} + H(\to t\bar{t})$	$pp \to t\bar{t}\,t\bar{t}$ + X	No
$Z + H(\to t\bar{t})$	$pp \to Zt\bar{t}$ + X estimated	No
$W + H(\to t\bar{t})$	$pp \to Wt\bar{t}$ + X and $Wtb + X$	Yes; further studies of resolution in $t\bar{t}$ invariant mass and t/b discrimination

Table VI.A - Continued

$(W,\ Z) + H(\rightarrow \tau^+\tau^-)$	$--$	Yes, for reconstructable W, Z modes (p_T^H measurable $\rightarrow m_H$ reconstructable.) Signal calculation with cuts, backgrounds of (W, Z) + $\tau^+\tau^-$, 2 jets + $\tau^+\tau^-$, 4 jets. Vertex detector desirable to assist in τ identification.
$t\bar{t} + H(\rightarrow \tau^+\tau^-)$	$--$	Perhaps, (seems less attractive than (W, Z) + $H(\rightarrow \tau^+\tau^-)$).
$(W, Z) + H(\rightarrow (W\bar{f}f'),\ (Z\bar{f}f))$	$--$	Yes, but only of potential use for 135 $GeV < m_H <$ 160 GeV (p_T^H measurable $\rightarrow m_H$ reconstructable in $Z\bar{f}f$ decay channel); signal with cuts, backgrounds e.g. listed in Fig's. (21(a)-(d)).
$t\bar{t} + H(\rightarrow (W\bar{f}f'),\ (Z\bar{f}f))$	$--$	Perhaps. (Seems less attractive than $(W, Z) + H(\rightarrow (Wff'),$ $(Z\bar{f}f))$

APPENDIX A

The first trick for computing $gg \to W^+bt$ involves the two three-gluon vertex diagrams of Fig. 8c. Typically the gluon vertices are expressed in terms of the momenta k_1 and k_2 of the incoming gluons as well as the momentum $(k_1 + k_2)$ of the s-channel gluon. At the amplitude level this vertex structure is dotted into physical gluon polarizations $\epsilon_1^\alpha(k_1)$ and $\epsilon_2^\beta(k_2)$. Terms proportional to k_1^α or k_2^β may be dropped by virtue of the relations, $\epsilon_2(k_2) \cdot k_2 = \epsilon_1(k_1) \cdot k_1 = 0$, yielding a reduced amplitude $\hat{M}_{\alpha\beta}$. It is straightforward to show that

$$k_1^\alpha \ \hat{M}_{\alpha\beta} = k_2^\beta \ \hat{M}_{\alpha\beta} = 0 \ . \tag{A.1}$$

Calculationally this occurs as follows. Defining a and b to be the respective color indices of gluons 1 and 2, the three gluon diagrams have a structure proportional to f^{abc}, while the six cross related quark exchange diagrams are proportional to T^aT^b and T^bT^a. In $k_1^\alpha \ \hat{M}_{\alpha\beta}$ or $k_2^\beta \ \hat{M}_{\alpha\beta}$ the T^aT^b and T^bT^a terms combine to yield a term proportional to f^{abc} which cancels that coming directly from the three-gluon diagrams. Thus in computing the matrix element squared and summing over polarizations we may drop the term proportional to k_1 and k_2 in

$$\begin{aligned} \Sigma_{helicities} \ \epsilon_1^\alpha(k_1)\epsilon_1^{*\alpha'}(k_1) &= -g^{\alpha\alpha'} + (k_1^\alpha \ldots \text{ or } k_1^{\alpha'} \ldots) \\ \Sigma_{helicities} \ \epsilon_2^\beta(k_2)\epsilon_2^{*\beta'}(k_2) &= -g^{\beta\beta'} + (k_2^\beta \ldots \text{ or } k_2^{\beta'} \ldots) \ , \end{aligned} \tag{A.2}$$

keeping only the $g^{\alpha\alpha'}$ and $g^{\beta\beta'}$ tensor structure.

A second simplification makes use of the overall gauge invariance of the full Feynman diagram sum. Structures of the type

$$(\not{p}_b - m_b) \cdot \not{A}(1 - \gamma_5) \ (\not{p}_t - m_t) \ , \tag{A.3}$$

where $q = p_t - p_b$ and p_b and p_t are some (possibly internal) b and t momenta, emerge from the $\frac{q_\mu q_\nu}{m_W^2}$ part of the W propagator when dotted into the γ matrix structure on a fermion line. We may use gauge invariance identities to make the replacement

$$\not{q}(1-\gamma_5) \to m_b(1-\gamma_5) - m_t(1+\gamma_5) \ . \tag{A.4}$$

Finally, various crossing symmetries may be employed to express one subset of terms in $\langle|M|^2\rangle$ in terms of another, thereby avoiding actually computing both.

To obtain rapid convergence of the integrations, especially for the background (IV.3), an appropriate form of the phase space and folding integrations must be used. We have found that the following technique yields rapid convergence while conveniently allowing cuts in y_W^L, y_H^L and $(p_T)_{min}$, the laboratory center-of-mass rapidities and transverse momentum of the W and H (or $t\bar{t}$ system). We employ

$$\frac{d\sigma}{ds_H} = \frac{1}{8(2\pi)^4} \int dy_W^L \int dy_H^L \int_1^{1/\tau_+} \frac{dz}{z^2} \frac{P}{\left(\frac{v_H}{1-w^2v_H^2} + \frac{v_W}{1-w^2v_W^2}\right)} \int \frac{d\Omega_{t\bar{t}}\beta_{t\bar{t}}}{8}$$
$$\frac{f_1(x_1)f_2(x_2)}{\hat{s}\sqrt{\hat{s}}}\ \theta(w_0 - |w|)\ \theta\left[\ y_0 - \left|y_H^L - \frac{1}{2}\ \ell n\left(\frac{1-v_Hw}{1+v_Hw}\right)\right|\ \right] \tag{A.5}$$
$$\langle|M|^2\rangle$$

where

$$v_H = \frac{P}{E_H} \qquad v_W = \frac{P}{E_W} \ ,$$
$$w = \frac{1}{2v_Hv_W}\left\{\ \coth(y_W^L - y_H^L)(v_H + v_W)\right. \tag{A.6}$$
$$\left. - \sqrt{[\coth(y_W^L - y_H^L)]^2(v_H+v_W)^2 - 4v_Hv_W}\ \right\}$$

(All quantities in Eqs. (IV.11) and (IV.12) except y_W^L, y_H^L refer to the parton–parton center–of–mass). The momentum P and energies E_H and E_W are given by

$$\begin{aligned} P &= \sqrt{\hat{s}^2 + m_W^4 + s_H^2 - 2m_W^2\hat{s} - 2s_H\hat{s} - 2m_W^2 s_H}/(2\sqrt{\hat{s}}) \ , \\ E_H &= \sqrt{P^2 + s_H}, \qquad E_W = \sqrt{P^2 + m_W^2} \ , \end{aligned} \tag{A.7}$$

and $\hat{s}$ is the parton–parton center-of-mass energy squared given by

$$\hat{s} = s_L/z \tag{A.8}$$

where s_L is the total laboratory center-of-mass energy squared. The relation between z and the standard τ variable is

$$z = \frac{1}{\tau} = \frac{1}{x_1 x_2} \ . \tag{A.9}$$

In Eq. (A.5) we compute x_1 and x_2 as

$$\begin{aligned} x_1 &= \sqrt{\frac{1}{z}}\, e^{y_L} \\ x_2 &= \sqrt{\frac{1}{z}}\, e^{-y_L} \ , \end{aligned} \tag{A.10}$$

where

$$y_L = y_W^L - \frac{1}{2}\, \ell n \left(\frac{1 + w v_W}{1 - w v_W} \right) \tag{A.11}$$

is the rapidity of the parton-parton system in the overall laboratory center-of-mass. The $t\bar{t}$ phase space factors $d\Omega_{t\bar{t}}$ and $\beta_{t\bar{t}}$ are defined in the $t\bar{t}$ center-of-mass

frame with

$$\beta_{t\bar{t}} = \sqrt{1 - \frac{4m_t^2}{s_H}} \ . \tag{A.12}$$

Finally, the limits of integration are specified by

$$\tau_+ = \frac{1}{s_L} \left((p_T^{min^2} + m_W^2)^{1/2} + (p_T^{min^2} + s_H)^{1/2} \right)^2 \tag{A.13}$$

$$y_0 = \ell n \sqrt{z} \ , \tag{A.14}$$

$$w_0 = \sqrt{1 - \frac{(p_T^{min})^2}{P^2}} \ , \tag{A.15}$$

with P defined in Eq. (A.7). The functions f_1 and f_2 are the parton distribution functions with momentum normalization in terms of $\int \ x \ f(x) \ dx$.

REFERENCES

1. For introductions to the standard model, see I. J. R. Aitchison and A. J. G. Hey, Gauge Theories in Particle Physics, Adam Hilger, Bristol, 1982; L. B. Okun, Leptons and Quarks, North-Holland, Amsterdam, 1981; C. Quigg, Gauge Theories of the Strong, Weak, and Electromagnetic Interactions, Benjamin/Cummings, Reading, Massachusetts, 1983.
2. S. Weinberg, PR D13(1976)974 and D19(1979)1277; L. Susskind, PR D20(1979)2619.
3. S. Dimopoulos and J. Ellis, N.P. B182(1981)505.
4. E. Witten, N.P. B185 (1981)513; S. Dimopoulos and H. Georgi, N.P. B193(1981)150; H. Haber and G. Kane, Phys. Report 117(1985)75.
5. J. Bagger, S. Dimopoulos, E. Masso, and M. H. Reno, SLAC-PUB-3441(1985).
6. S. Weinberg, PRL36(1976)294; A. D. Linde, Pis'ma Zh.E.T.P. 23(1976)73.
7. B. W. Lee, C. Quigg, H. B. Thacker, PR D16(1977)1519.
8. See for example ECFA/LEP Specialized Study Group 9 Report, 'Production and Detection of Higgs Particles at LEP', G. Barbiellini, et.al.
9. See Ref. 7; B. L. Ioffe and V. A. Khoze, Leningrad Report No. LINP-274, 1976 (unpublished); J. Ellis, M. K. Gaillard, and D. V. Nanopoulos, N. P. B106(1976)292.
10. E. Eichten, I. Hinchliffe, K. Lane, and C. Quigg, RMP56(1984)579 and Supplement, presented at 1984 Summer Study on Design and Utilization of SSC, Snowmass, CO, Jun 23-Jul 13, 1984.
11. H. E. Haber, G. L. Kane, and T. Sterling, N.P. B161(1979)493.

12. H. M. Georgi, S. L. Glashow, M. E. Machacek, and D. V. Nanopoulos, PRL 40(1978)692.

13. R. W. Brown and K. O. Mikaelian, PR D19(1979)922.

14. Letter of Intent, CERN-LEP-LI-(4).

15. H. E. Haber and J. F. Gunion, SLAC-PUB-3404.

16. Z. Kunszt, N. P. B247(1984)339.

17. S. L. Glashow, D. V. Nanopoulos, and A. Yildiz, PR D18(1978)1724.

18. J. F. Gunion, P. Kalyniak, M. Soldate, and P. Galison, PRL 54(1985)1226, and SLAC-PUB-3414, presented at 1984 Summer Study on Design and Utilization of SSC, Snowmass, CO, Jun 23-Jul 13, 1984.

19. B. Cox, et.al., SLAC-PUB-3507, contributed to 1984 Summer Study on Design and Utilization of SSC, Snowmass, CO, Jun 23-Jul 13, 1984.

20. W.-Y. Keung and W. J. Marciano, PR D30(1984)248. We are in agreement with the results presented there for $\Gamma(H \to W\bar{f}f')$ and $\Gamma(H \to Z\bar{f}f)$.

21. A. I. Vainshtein, M. B. Voloshin, V. I. Zakharov, and M. A. Shifman, Yad. Fiz. 30(1979)1368; See J. Ellis, et.al, Ref. 9 for a calculation of $\Gamma(H \to \gamma\gamma)$ valid to lowest order in M_H^2/M_W^2.

22. R. N. Cahn, M. S. Chanowitz, and N. Fleishon, PL 82B(1979)113. We performed a numerical integration of Eq. 12 in this reference to arrive at Eq. (V.11) of the present paper.

23. We thank F. Halzen for suggesting that the $\tau^+\tau-$ decay of H in associative production could be of interest. See V. Barger, F. Halzen, and W. Y. Keung, Phys.Rev. D25(1982)1838.

24. S. S. D. Willenbrock and D. A. Dicus, UTTG-03-85.

25. J. F. Gunion, Z. Kunszt, and M. Soldate, Phys. Lett. B163, 389(1985) and erratum thereto. S. D. Ellis, R. Kleiss, and J. Stirling, Phys. Lett. B163, 261(1985).

26. We thank F. E. Paige for the comment that follows in the text.

FIGURE CAPTIONS

1. Feynman diagrams for

   (*a*) $e^+e^- \to Z^* \to ZH(\to t\bar{t})$ and

   (*b*) $e^+e^- \to Zt\bar{t}$ continuum production.

2. The diagrams for continuum production of $Zt\bar{t}$ which dominate when $(p_t + p_{\bar{t}})^2 \approx m_Z^2$.

3. (a) $\Sigma_{SIG}(s_o, \Delta s_H)$ for $\Delta s_H = .02 s_o$, $m_H = 93$ GeV, and $\sqrt{s} = 300$ GeV.

   (*b*) The curve $\cdots\cdots$ is $\Sigma_{SIG}(s_o, \Delta s_H)|_{(m_H^2 = s_o)}$. The curves ——, − − −, and − · − · are $\Sigma_{BG}^{Z-pole}(s_o, \Delta s_H)$ when the final state $q\bar{q}$ pair is $t\bar{t}$; $t\bar{t}$ or $b\bar{b}$; $t\bar{t}$, $b\bar{b}$, $c\bar{c}$, $s\bar{s}$, $u\bar{u}$, or $d\bar{d}$ respectively. $\Delta s_H = .02 s_o$, $\sqrt{s} = 300$ GeV.

4. (a) The curves − · − , − ·· − ··, and $\cdots$ are $\Sigma_{BG}(s_o, \Delta s_H)$ calculated from the sum of the terms proportional to $A^2 + B^2$, $C^2 + D^2$, and AC + BD in Eq. (II.20) when the final state $q\bar{q}$ pair is $t\bar{t}$; $t\bar{t}$ or $b\bar{b}$; $t\bar{t}$, $b\bar{b}$, $c\bar{c}$, $s\bar{s}$, $u\bar{u}$, or $d\bar{d}$ respectively. For comparison the curves − ··· − ···, ——, and − − − are $\Sigma_{BG}(s_o, \Delta s_H)$ calculated from the terms proportional to $A^2 + B^2$ (in other words Σ_{BG}^{Z-pole}) in Eq. (II.20) when the final state $q\bar{q}$ pair is $t\bar{t}$; $t\bar{t}$ or $b\bar{b}$; $t\bar{t}$, $b\bar{b}$, $c\bar{c}$, $s\bar{s}$, $u\bar{u}$, or $d\bar{d}$, respectively. $\Delta s_H = .02\ \ s_o$ throughout, $\sqrt{s} = 300$ GeV.

   (*b*) $\Sigma_{SIG}(s_o, \Delta s_H)$ evaluated at $(m_H^2 = s_o)$ for $\Delta s_H = .02 s_o$, $\sqrt{s} = 300$ GeV.

5. The curve —— is $\Sigma_{BG}(s_o, \Delta s_H)$ calculated for the terms proportional to $A^2 = B^2$, $C^2 + D^2$, and AC + BD in Eq. (II.20), while the curve − − − − is $\Sigma(s_o, \Delta s_H)$ calculated from the terms proportional to EC + FD. The

final state $q\bar{q}$ pair is $t\bar{t}$ only. $\Delta s_H = .02\ s_\circ$.

6. Feynman diagrams for

   (*a*) $gg \to H^0 \to t\bar{t}$ via quark loop

   (*b*) $gg \to t\bar{t}$ continuum production.

7. Feynman diagram for

   (*a*) $q\bar{q} \to ZH^0(\to t\bar{t})$

   (*b*) $q\bar{q}$ or $gg \to Zt\bar{t}$ continuum production.

8. Feynman diagrams for

   (*a*) $u\bar{d} \to W^{+*} \to W^+H^o(\to t\bar{t})$,

   (*b*) $u\bar{d} \to W^+t\bar{t}$ continuum production, and

   (*c*) $gg \to W^+b\bar{t}$ continuum production.

9. – 14. Captions are contained in the text of Section IV.

15. Branching ratios for H^0 into the modes indicated as a function of m_H. $m_t =$ 40 GeV.

16. The curve – – ––, is $\Sigma_{BG}(\tau^+\tau^-)$, —— is $\Sigma_{SIG}(\tau^+\tau^-)$ as a function of m_H^2. $\Delta s_H = .1\ m_H^2$.

17. The curves ———, – · · – · · , and – · · · – · · · are $\Sigma_{BG}(\tau^+\tau^-)$ for m_H = 100, 130, and 160 GeV respectively. The curves – – – , – · – · , and · · · · · are $\Sigma_{SIG}(\tau^+\tau^-)$ for m_H^2 = 100, 130, and 160 GeV respectively. All are shown as functions of the mass, m_L, of the new heavy lepton. $\Delta s_H = .1 m_H^2, \sqrt{s} = 40\ TeV$.

18. The curves – · – · , – · · are $\Sigma_{BG}(\gamma\gamma)$ and $\Sigma_{SIG}(\gamma\gamma)$ respectively. The curves · · · · · , —— are $\Sigma_{BG}(\gamma Z)$ and $\Sigma_{SIG}(\gamma Z)$ respectively. $\Delta s_H =$ $.02 m_H^2, \sqrt{s} = 40$ TeV.

19. The curves – – – and ——, are $\widetilde{\Sigma}_{SIG}(W\bar{f}f')$ and $\widetilde{\Sigma}_{SIG}(Z\bar{f}f)$ respectively, summed over W^+, W^-, and light fermion final states. $\sqrt{s} = 40$ TeV.

20. Typical Feynman graph for $gg \to q_1\bar{q}_2\ \ell\bar{\nu}_\ell$.

21. Typical Feynman graphs for

    (*a*) $q\bar{q} \to S_1\ S_1\ S_2$,

    (*b*) $gg \to q_1\bar{q}_1\ S_2$, and (S_1 or S_2),

    (*c*) $q\bar{q} \to S_1 S_2$ and (S_1 or S_2)

    (*d*) $q\bar{q} \to S_2(S_1$ or $S_2)$ and (S_1 or S_2).

The sets S_1 and S_2 are specified by Eqs. (V.43) and (V.44).

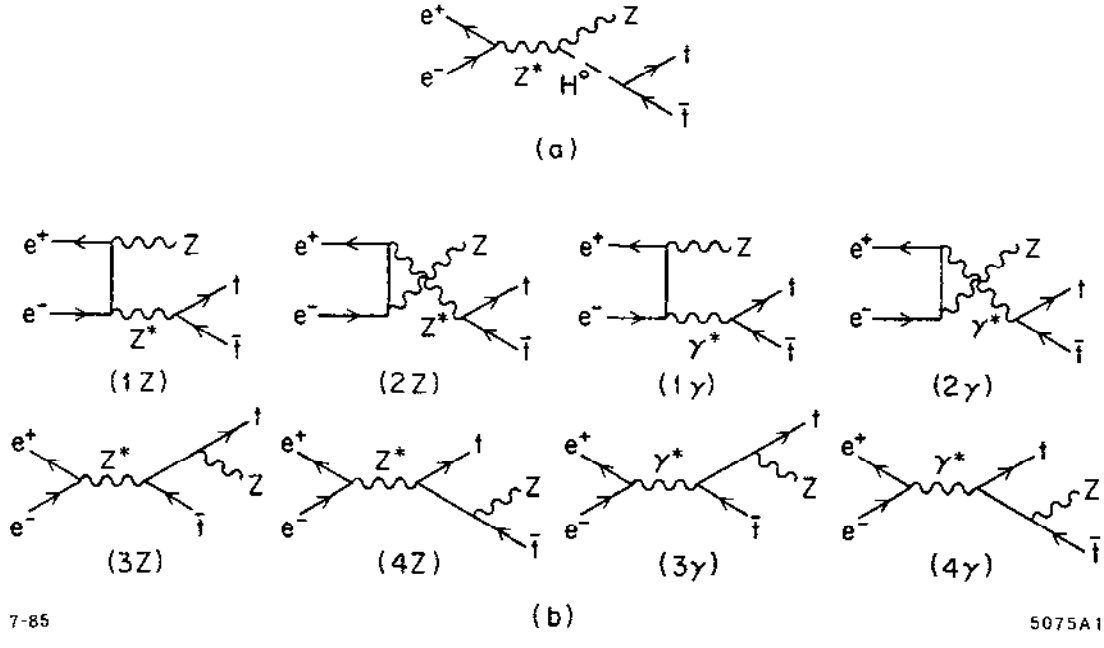

Fig. 1

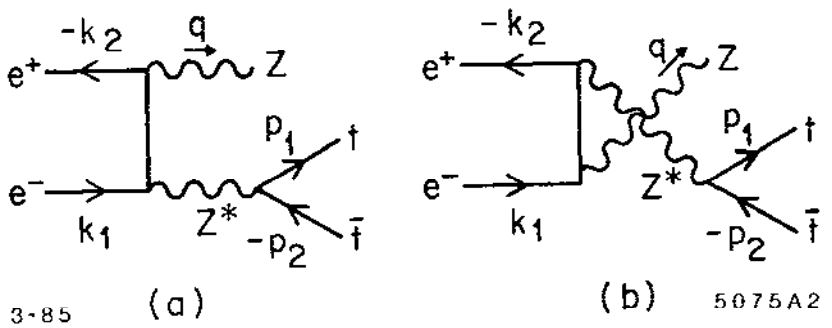

Fig. 2

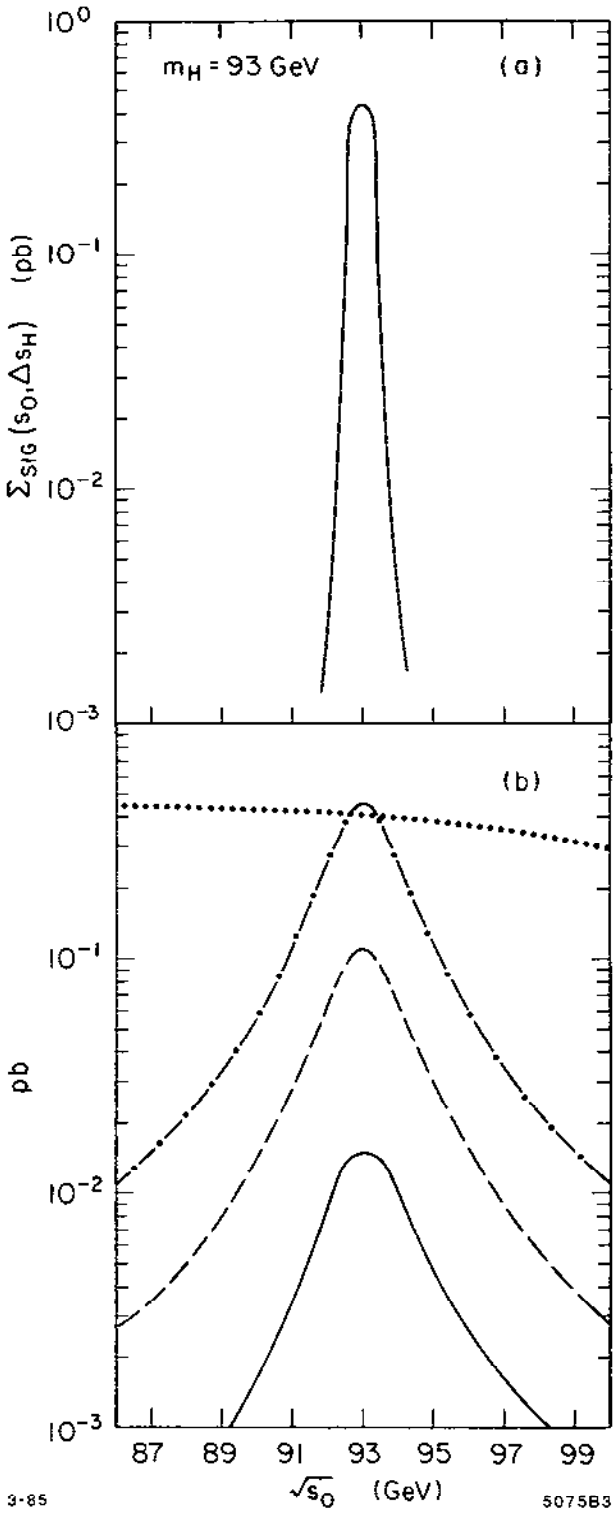
m_H = 93 GeV
(a)
(b)
$\Sigma_{SIG}(s_0,\Delta s_H)$ (pb)
pb
10^0
10^{-1}
10^{-2}
10^{-3}
87
89
91
93
95
97
99
$\sqrt{s_0}$ (GeV)
3-85
5075B3

Fig. 3

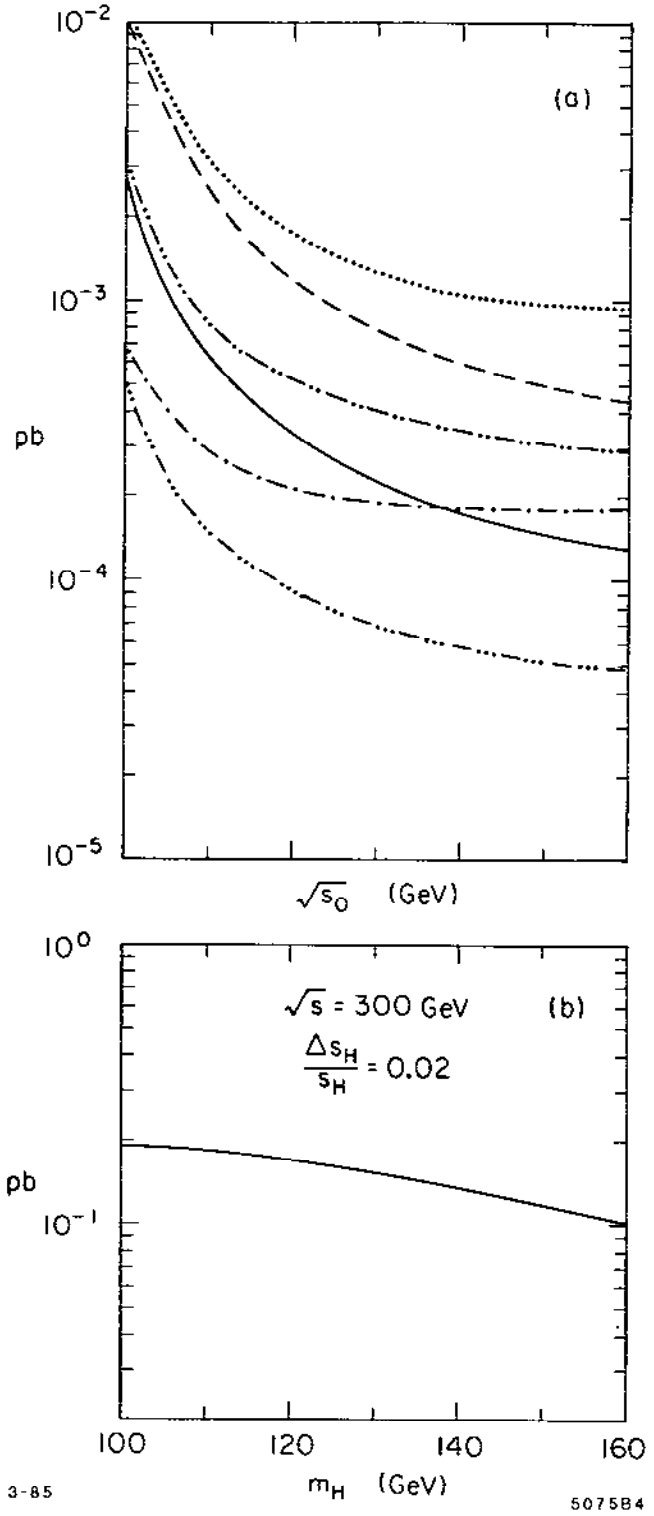
10^{-2}
(a)
10^{-3}
pb
10^{-4}
10^{-5}
$\sqrt{s_0}$ (GeV)
10^{0}
$\sqrt{s}$ = 300 GeV
(b)
$\frac{\Delta s_H}{s_H}$ = 0.02
pb
10^{-1}
100
120
140
160
m_H (GeV)
3-85
5075B4

Fig. 4

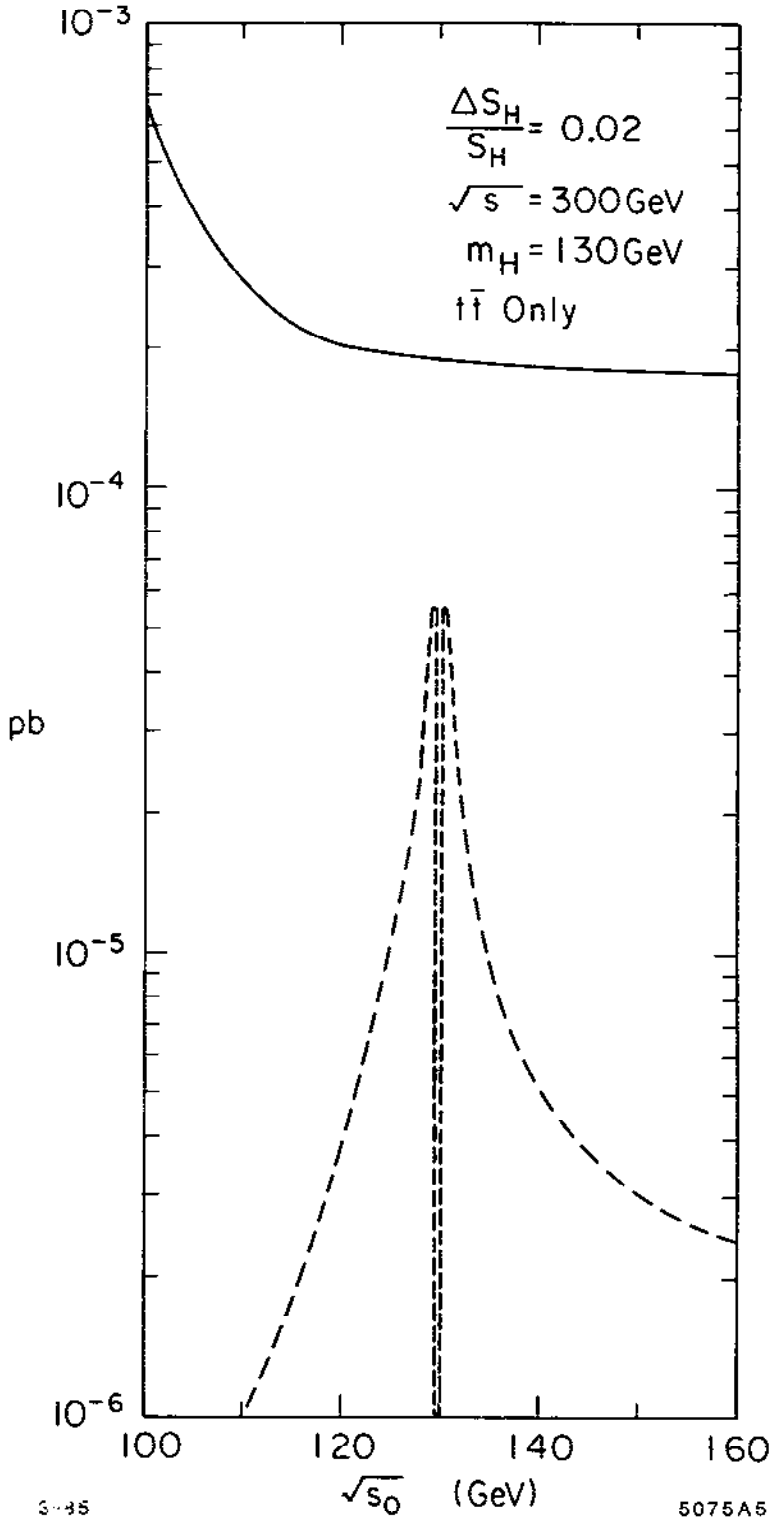
10^{-3}
10^{-4}
10^{-5}
10^{-6}
pb
$\frac{\Delta S_H}{S_H} = 0.02$
$\sqrt{s} = 300\,GeV$
$m_H = 130\,GeV$
$t\bar{t}$ Only
100
120
140
160
$\sqrt{s_0}$ (GeV)
3-85
5075A5

Fig. 5

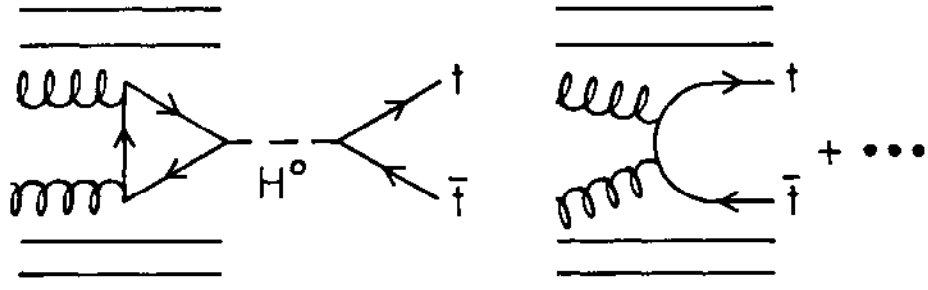

Fig. 6

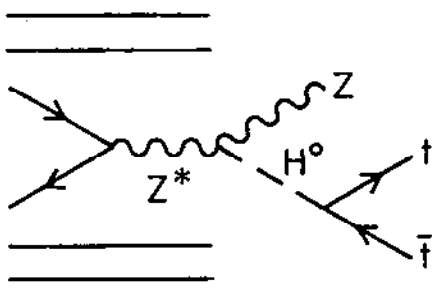

(a)

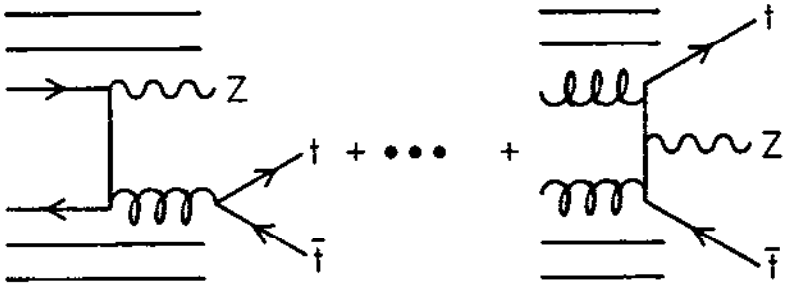

3-85 (b) 5075A7

Fig. 7

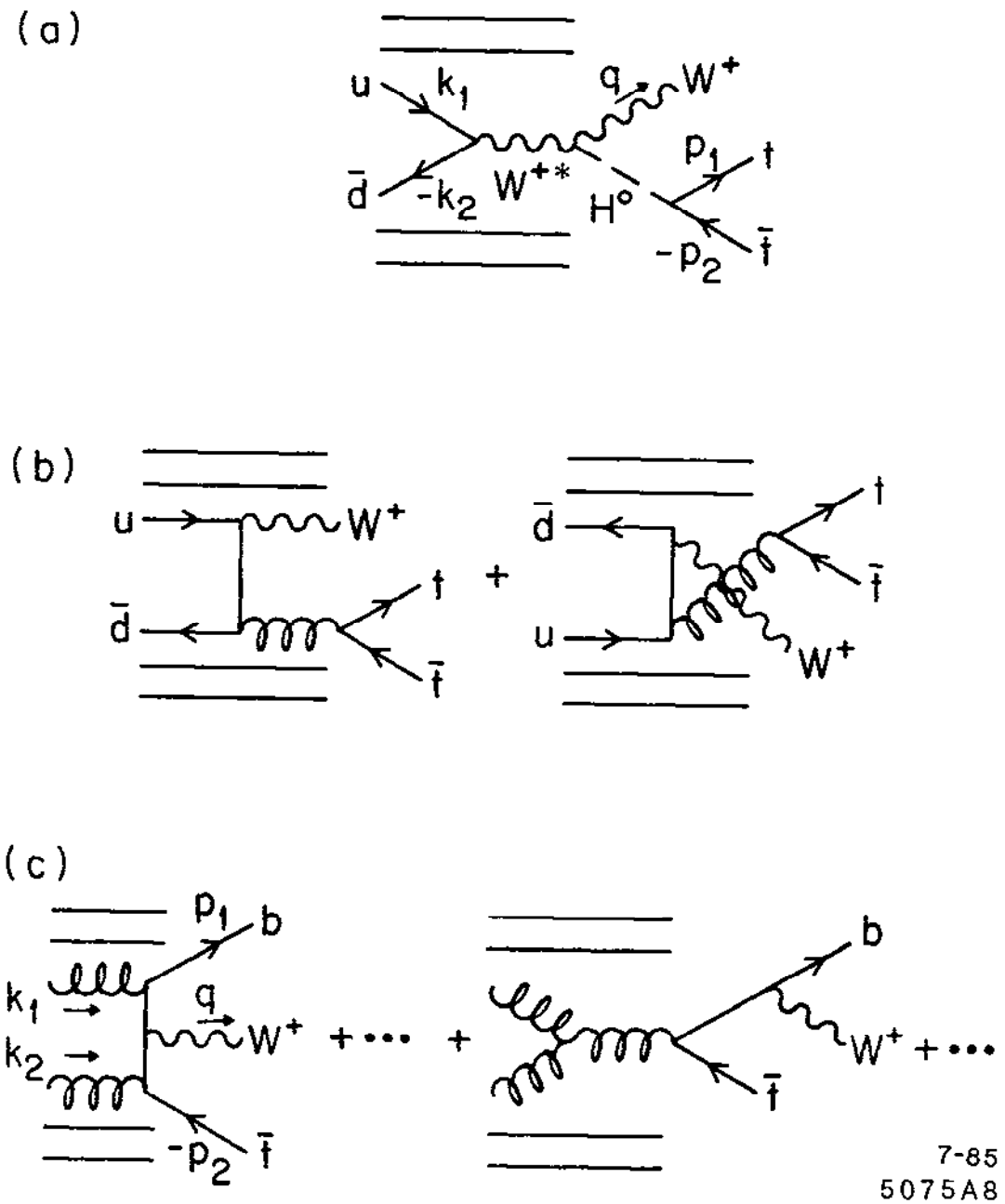
(a)
u
k_1
q
W^+
p_1
t
$\bar{d}$
$-k_2$
W^{+*}
H^0
$-p_2$
$\bar{t}$
(b)
u
W^+
$\bar{d}$
t
$\bar{t}$
+
$\bar{d}$
t
$\bar{t}$
u
W^+
(c)
p_1
b
k_1
q
W^+ +••• +
k_2
$-p_2$
$\bar{t}$
b
W^+ +•••
$\bar{t}$
7-85
5075A8

Fig. 8

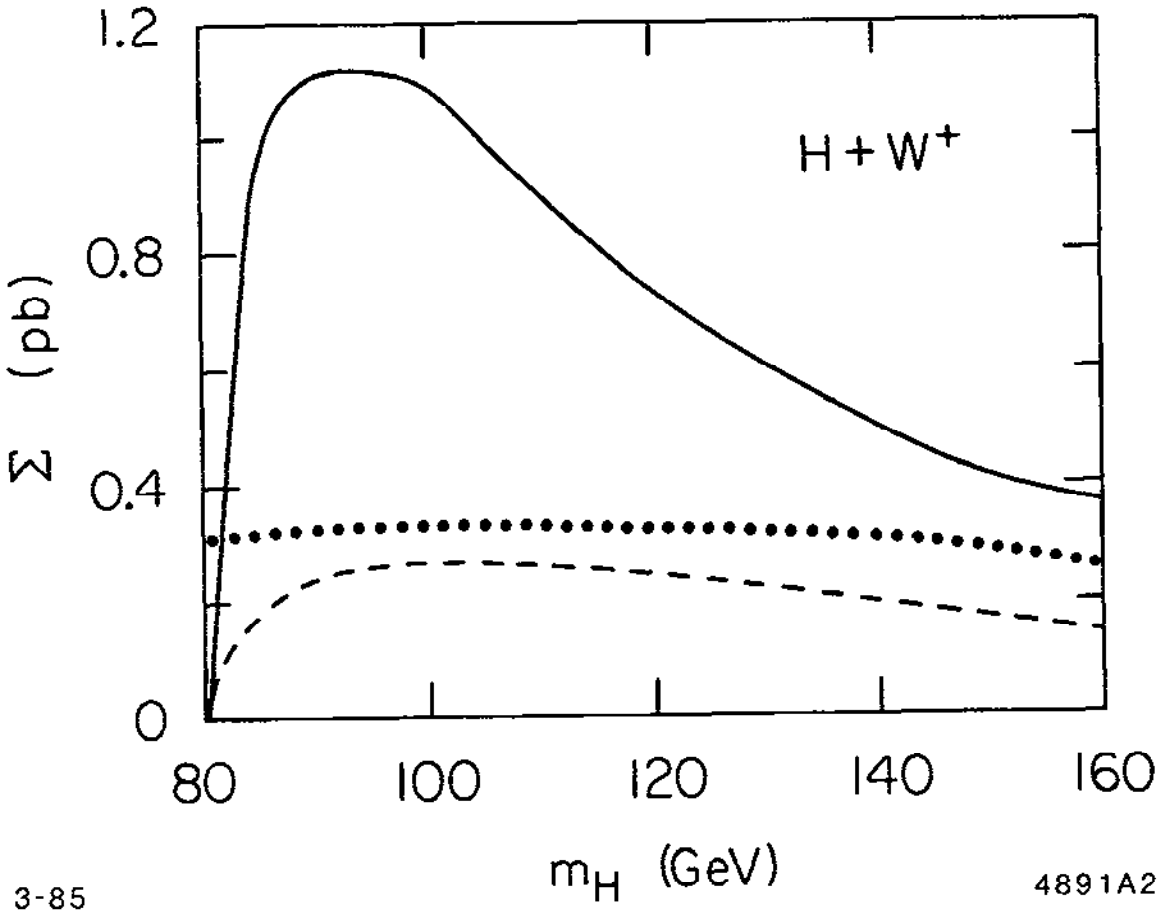

Fig. 9

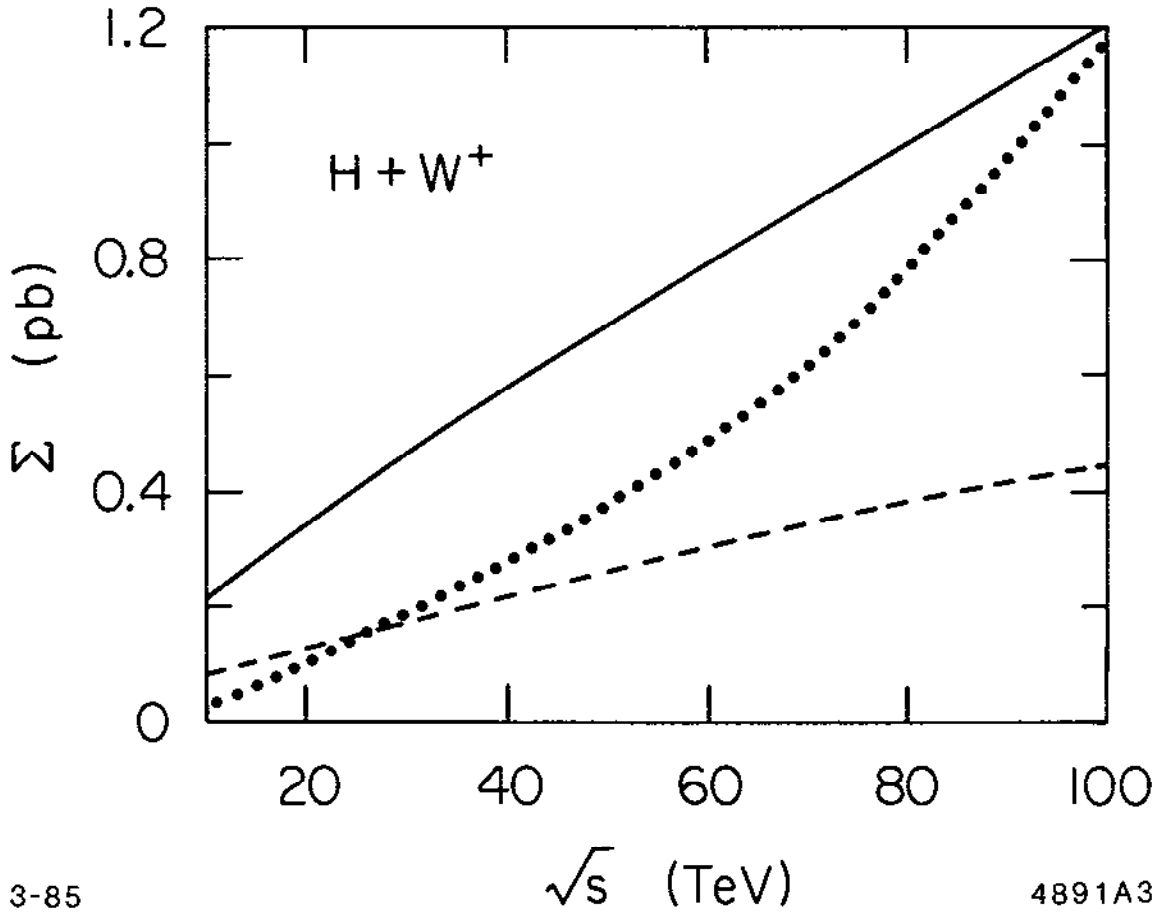

Fig. 10

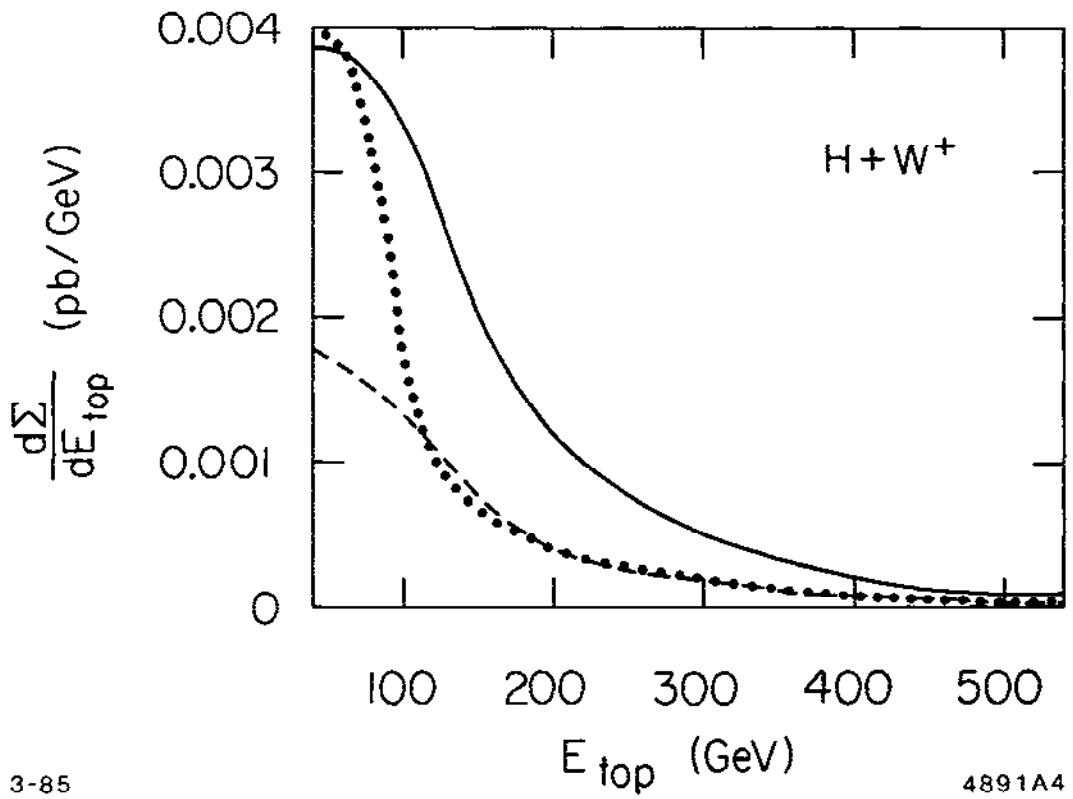
0.004
0.003
0.002
0.001
0
$\frac{d\Sigma}{dE_{top}}$ (pb/GeV)
H+W+
100
200
300
400
500
E top (GeV)
3-85
4891A4

Fig. 11

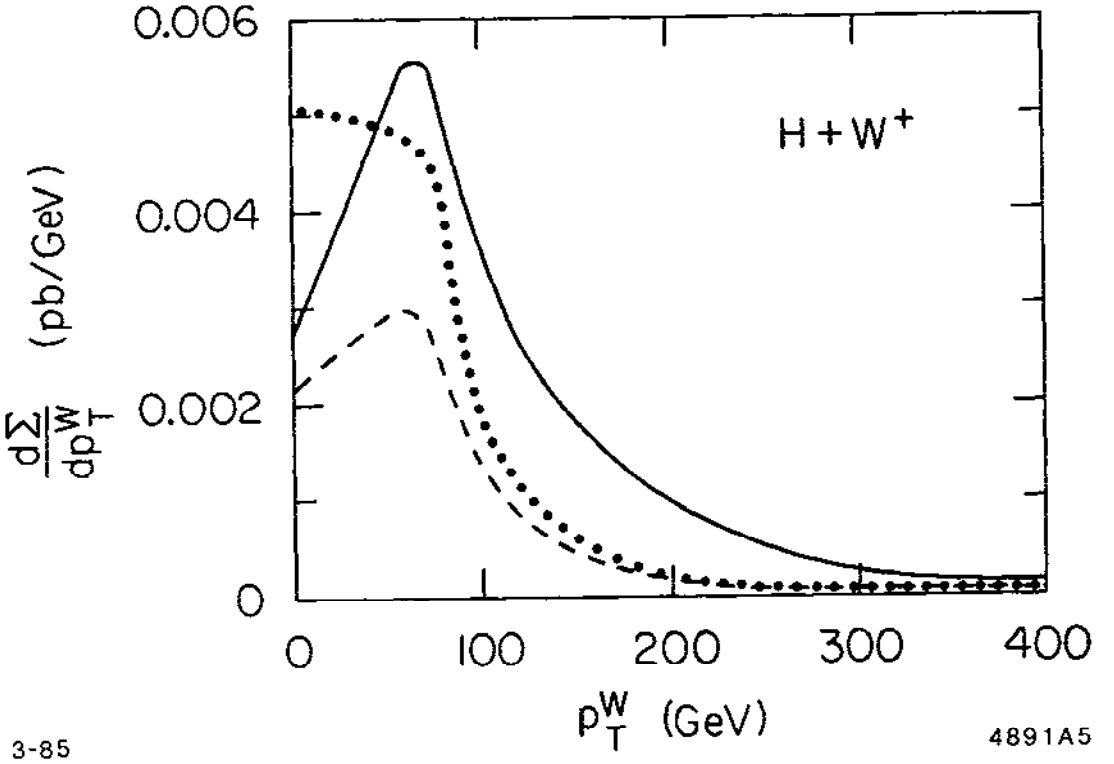
0.006
0.004
0.002
0
H + W+
$\frac{d\Sigma}{dp_T^W}$ (pb/GeV)
0
100
200
300
400
p_T^W (GeV)
3-85
4891A5

Fig. 12

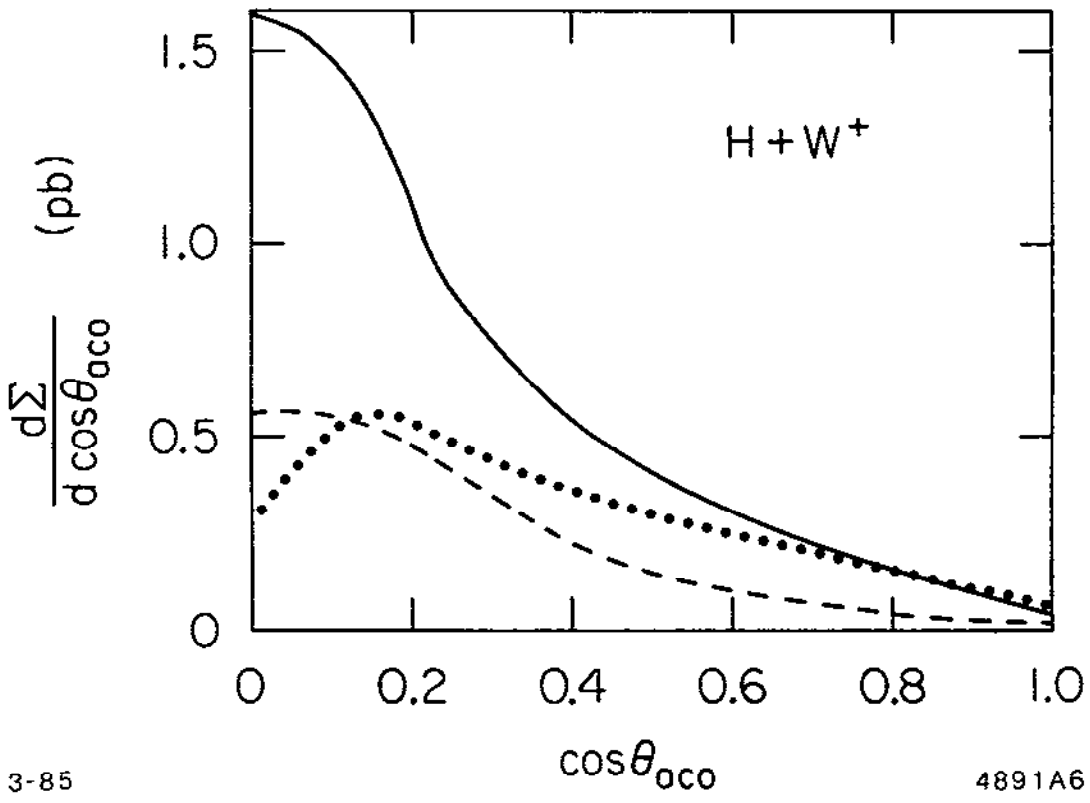

Fig. 13

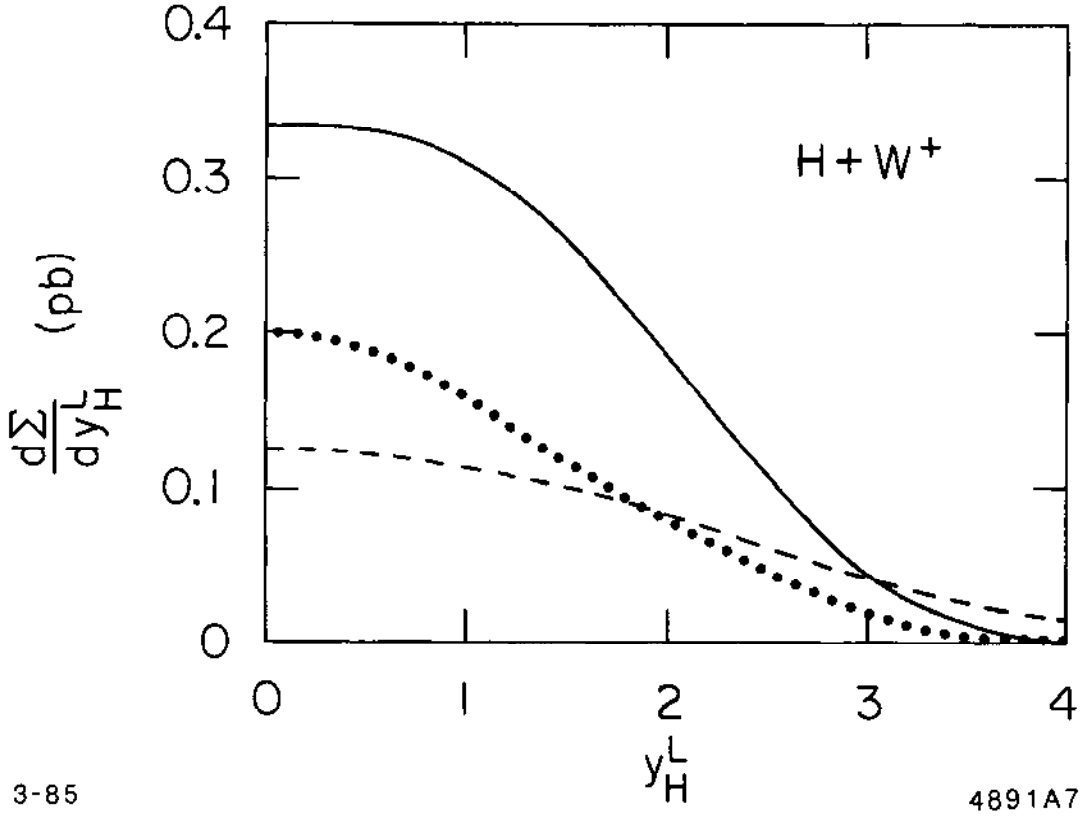

Fig. 14

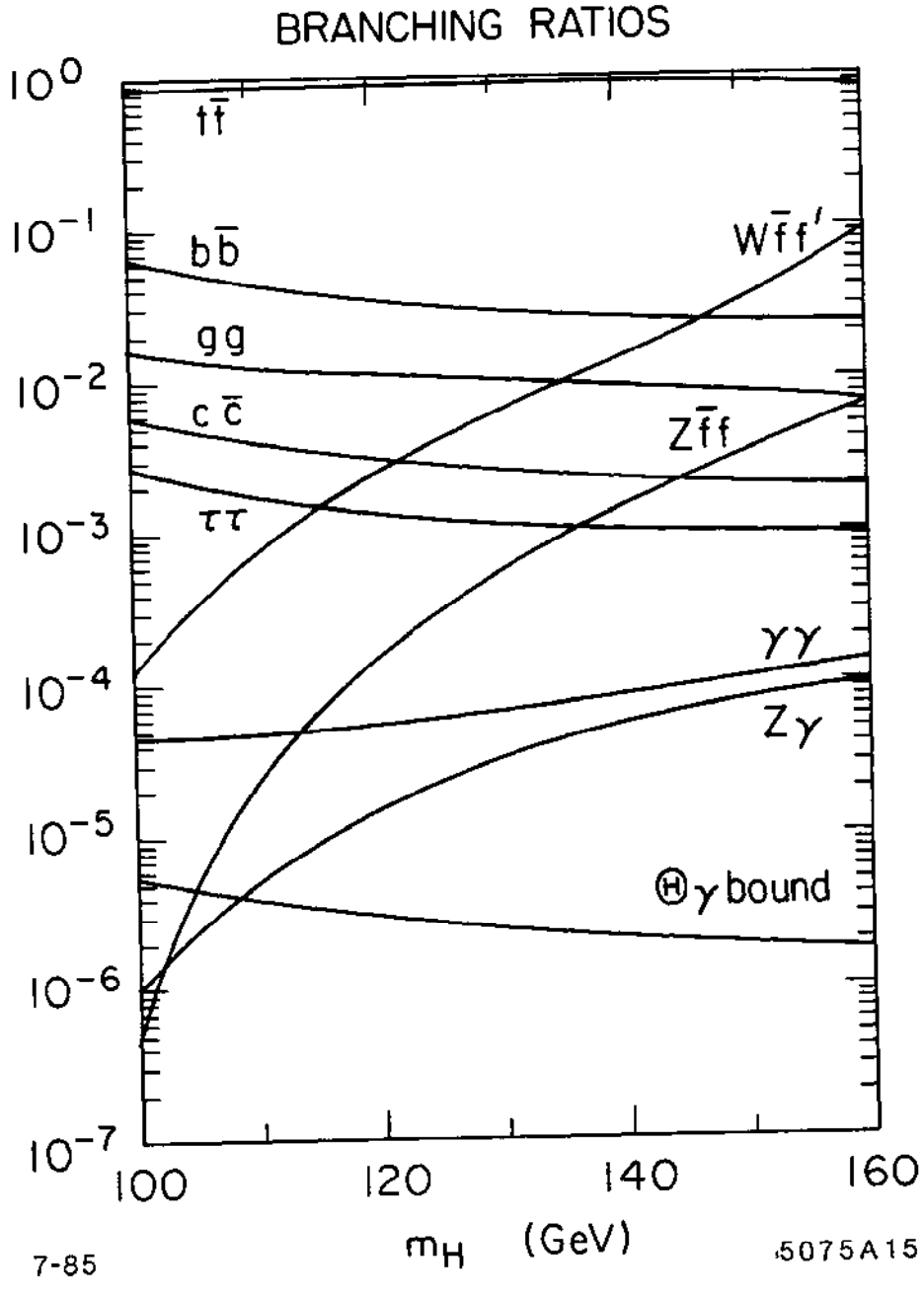
BRANCHING RATIOS
10^0
10^{-1}
10^{-2}
10^{-3}
10^{-4}
10^{-5}
10^{-6}
10^{-7}
$t\bar{t}$
$b\bar{b}$
gg
$c\bar{c}$
$\tau\tau$
$W\bar{f}f'$
$Z\bar{f}f$
$\gamma\gamma$
$Z\gamma$
Ⓗγ bound
100
120
140
160
m_H (GeV)
7-85
5075A15

Fig. 15

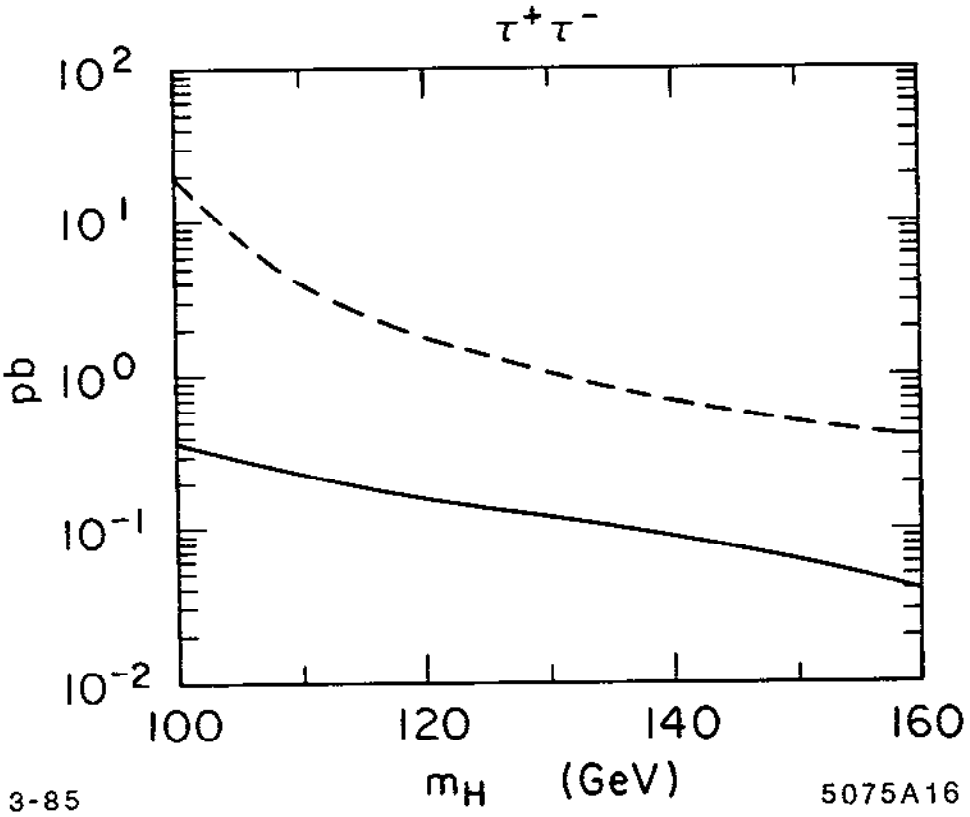
$\tau^+\tau^-$
10^2
10^1
10^0
10^{-1}
10^{-2}
pb
100
120
140
160
m_H (GeV)
3-85
5075A16

Fig. 16

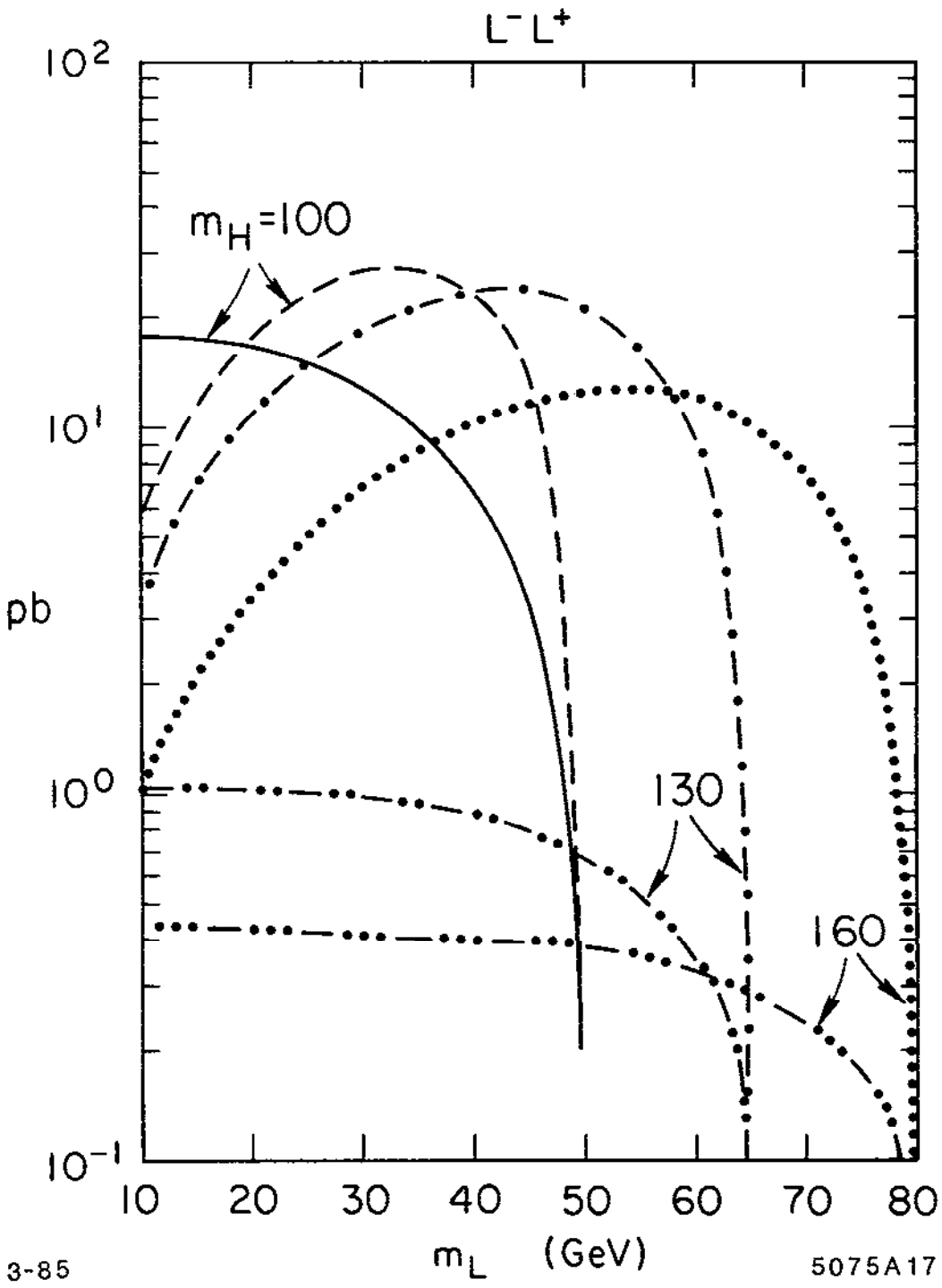
L⁻L⁺
10²
10¹
10⁰
10⁻¹
pb
m_H=100
130
160
10
20
30
40
50
60
70
80
m_L (GeV)
3-85
5075A17

Fig. 17

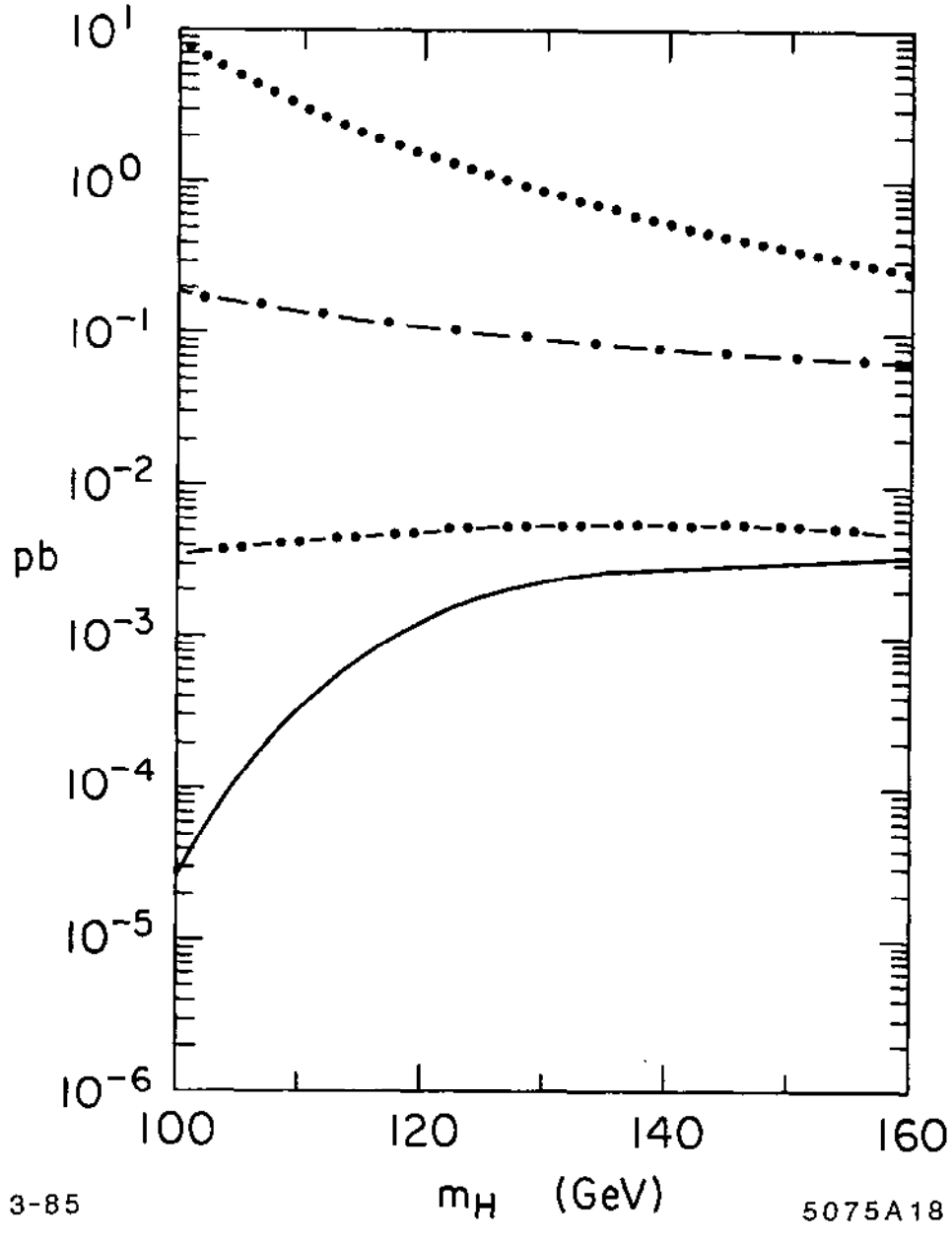
10^1
10^0
10^{-1}
10^{-2}
pb
10^{-3}
10^{-4}
10^{-5}
10^{-6}
100
120
140
160
m_H (GeV)
3-85
5075A18

Fig. 18

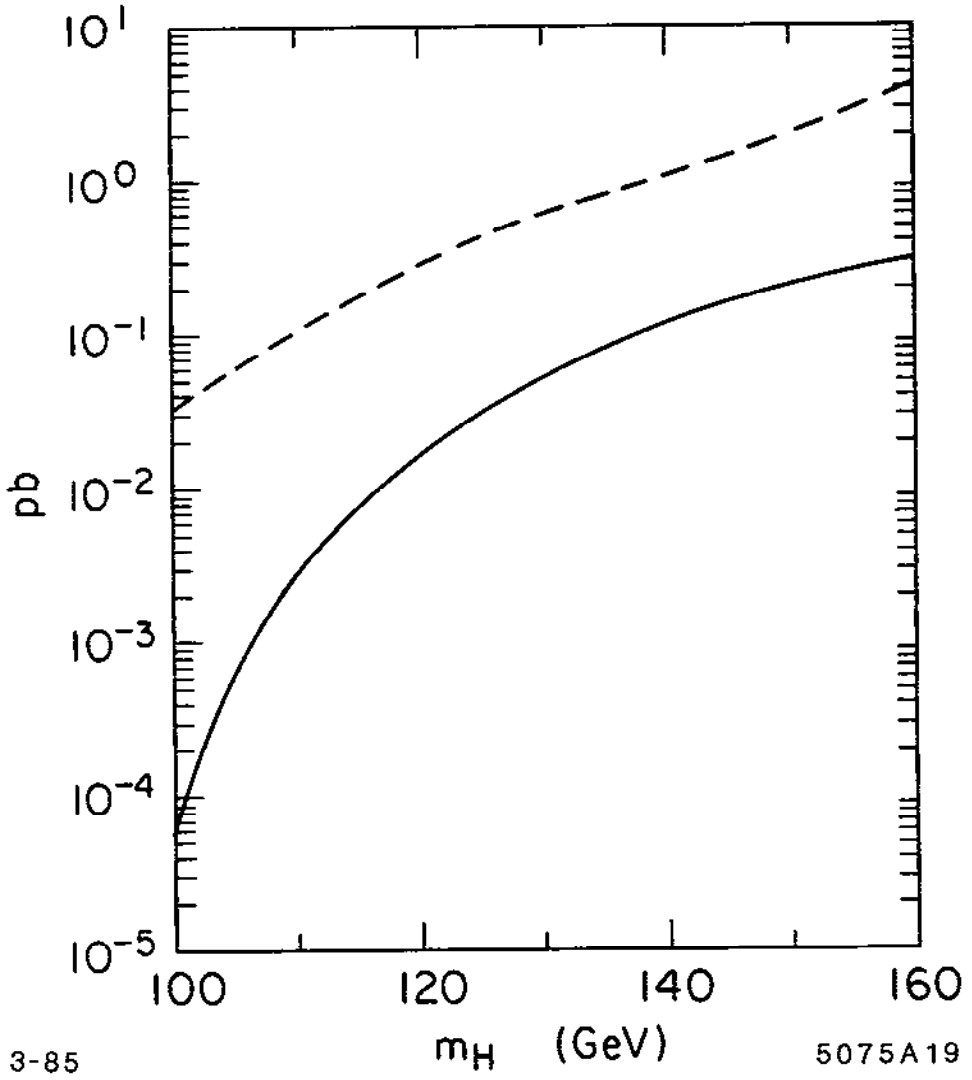
10^1
10^0
10^{-1}
10^{-2}
10^{-3}
10^{-4}
10^{-5}
pb
100
120
140
160
m_H (GeV)
3-85
5075A19

Fig. 19

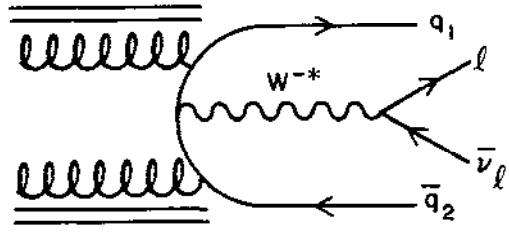

3-85 5075A21

Fig. 20

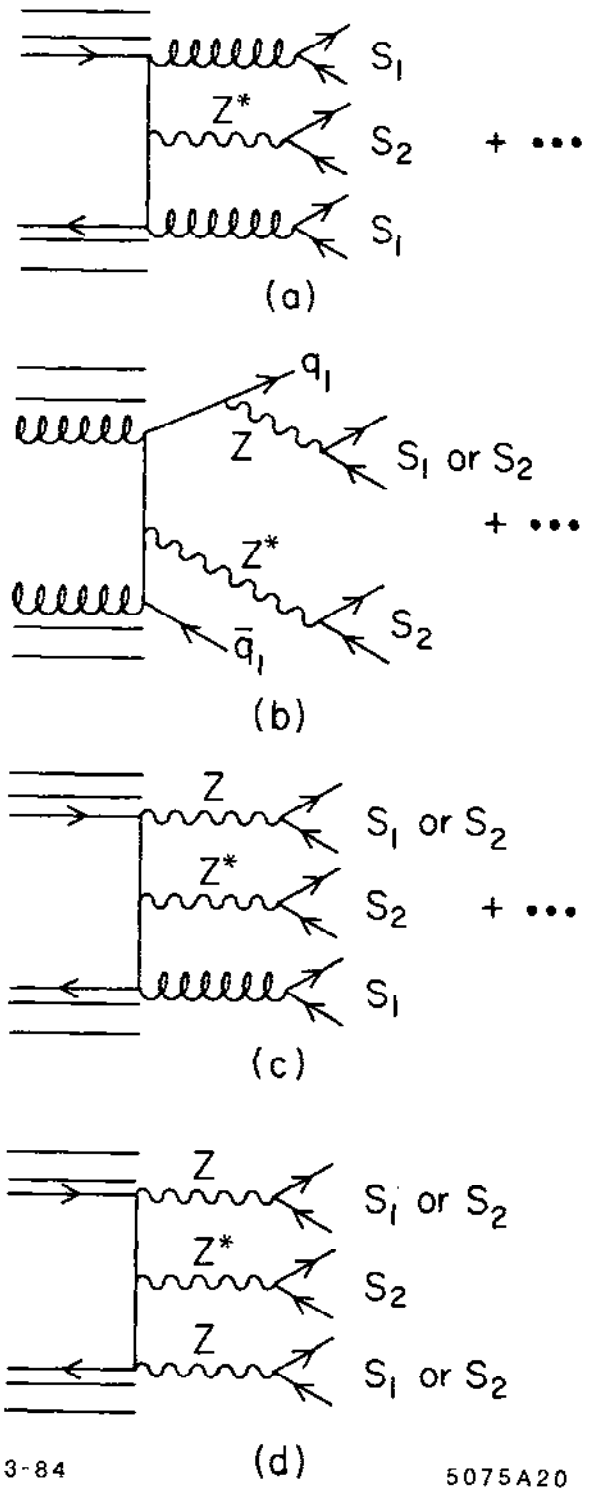
S_1
Z^*
S_2
+ •••
S_1
(a)
q_1
Z
S_1 or S_2
+ •••
Z^*
S_2
$\bar{q}_1$
(b)
Z
S_1 or S_2
Z^*
S_2
+ •••
S_1
(c)
Z
S_1 or S_2
Z^*
S_2
Z
S_1 or S_2
(d)
3-84
5075A20

Fig. 21